EARLY DETECTION OF METASTATIC CANCER USING COMPUTATIONAL ANALYSIS

by

NUZHAT MANSUR

Presented to the Faculty of the Graduate School of

The University of Texas at Arlington in Partial Fulfillment

of the Requirements

for the Degree of

DOCTOR OF PHILOSOPHY

THE UNIVERSITY OF TEXAS AT ARLINGTON

August 2017

Acknowledgements

I would like to express my gratitude to my family for their continuous support and encouragement. My parents, who always stood by me; my brother and sister-in-law, who without hesitation took care of my share of responsibilities; my in-laws, who always pushed me to pursue my dreams-were and are the source of my strength and energy. I am extremely fortunate that Dr. Samir Iqbal gave me the opportunity to explore my passion for research. His guidance and expertise have enabled me to steer through the hard and intense moments of a researcher's life. I would like to specially thank Dr. Young-tae Kim for his generous help. Dr. Arif I. Mahmood, Dr. Muhymin Islam, Dr. Loan Bui, Muhammad Usman Raza, Mohammad Abdallah, Sai Santosh Sasank Peri, the faculty and staff of Department of Electrical Engineering and Nanotechnology research center have helped me immensely for which I am forever grateful. Friends in Arlington will always hold a dear place in my heart for making my graduate life full of fun and excitement. Lastly, I would like to thank Razi for always being there for me, nothing would not have been possible without you.

August 22, 2017

Abstract

Early Detection of Metastatic Cancer using Computational Analysis

Nuzhat Mansur, PhD

University of Texas at Arlington, 2017

Supervising Professor: Samir M. Iqbal

Metastasis is the leading cause of cancer related deaths. Early detection of cancer cells can enable early disease diagnosis and stage specific therapeutics. Metastatic cancer cells have abnormal expression of certain proteins. One such protein is Epidermal Growth Factor Receptor (EGFR). Anti-EGFR aptamers have emerged as more effective probe molecules for selectively binding with EGFR compared to antibodies. Capturing cancer cells with aptamer is an emerging and developing technique for cancer cell isolation. Nanotextured substrates inspired by naturally occurring basement membranes are promising platform for triggering unique cell behavior. Along with the biochemical and physical techniques to probe cancer cell behavior, mathematical analysis using high performing computers is proving to be highly efficient for accurate and fast inference. This work is presented with the anticipation of presenting a novel and exciting approach based on computational analysis of cellular behavior on physically and biochemically modified substrates to detect metastatic cancer cells at early stage.

This research focuses on two major areas. One is observing, understanding and modifying cellular behavior on functionalized substrates. The other focus is utilizing the developed platform for cancer detection similar to a clinical setting and ultimately pave the path for a future point of care device.

Table of Contents

List of Illustrations

List of Tables

Chapter 1

INTRODUCTION

1.1. Research Objective

Cancer is a fatal disease and a major health hazard. It is the uncontrolled growth of cells which can penetrate adjacent tissue and travel through circulatory system to reach other organs. This process, called metastasis, creates new cancer in the distant organs. Early cancer diagnosis is crucial for preventing metastasis. Current techniques are proving to be not sufficiently efficient for detecting cancer at early stages. Detection techniques to capture and isolate cancer cells from biopsy or bodily fluids are being researched extensively. Detection of cancer cells requires high selectivity and acute sensitivity. The focus of this dissertation is to develop a detection platform towards a future point of care device for early detection of metastatic cancer.

1.2. Overview of Research Work

In chapter 2, we have reviewed the current clinical and laboratory techniques to detect cancer cells. In the following chapters our research works for detecting metastatic cancer cells are described.

1.2.1. Discrimination of Metastatic Breast Cancer Cells from Indolent Cells on Aptamer Functionalized Surface with Imaging Based Contour Following Techniques

Early detection of metastatic cells can lead to better prognosis and higher survival rate of patients. Often the symptoms for metastasis are not evident till cancer incapacitates a secondary organ. Early detection is the key to prevent metastasis. In chapter 3, an

imaging based approach with contour detection technique is presented to distinguish metastatic breast cancer cells from benign cells when captured on anti-EGFR aptamer modified glass substrates. The metastatic (MDA-MDB-231) and non-metastatic (MCF-7) breast cancer cells were studied. Temporal tracking of cells showed that metastatic cells depicted prominent morphological change whereas the benign cells did not show such behavior. Metastatic cells showed rapid change in shape by protruding/retracting cell membrane. Images of each type of cells captured on functionalized substrates were analyzed and morphology changes were quantified. Low similarity coefficient meant more morphology change and metastatic cells showed low similarity coefficient. High distance values meant more morphology change. Metastatic cells showed higher distance matrix values (average Hausdorff distance=2.8 a.u.; average Mahalanobis distance=0.7 a.u.) than non-metastatic cells (average Hausdorff distance=1.5 a.u.; average Mahalanobis distance=0.31 a.u.). These parameters were successfully used to detect 52% metastatic cells in a cell mixture that imitated breast tissue. This approach can be used for detecting metastatic potential of a given sample towards precise therapy for a patient.

1.2.2. Functionalization of Nanotextured Substrates for Enhanced Identification of Metastatic Breast Cancer Cells

In chapter 4, we report a nanotextured platform for enhanced detection of metastatic cells. We captured metastatic (MDA-MDB-231) and non-metastatic (MCF-7) breast cancer cells on anti-EGFR aptamer modified plane and nanotextured substrates. Metastatic cells were seen to change their morphology at higher rates when captured on nanotextured substrates than on plane substrates. Analysis showed statistically different morphological behaviors of metastatic cells that were much pronounced on nanotextured substrates.

Several distance matrices were calculated to quantify dissimilarity of cell shape change. Nanotexturing increased dissimilarity of metastatic cells, as a result the contrast between metastatic and non-metastatic cells increased. Jaccard distance measured that non-metastatic and metastatic cell shape change ratio enhanced from 1:1.01 to 1:1.81, going from plane to nanotextured substrates. Non-metastatic to metastatic cell shape change ratio improved from 1:1.48 to 1:2.19 for Hausdorff distance and from 1:1.87 to 1:4.69 for Mahalanobis distance after introducing nanotexture. Distance matrix analysis showed that nanotexture amplified shape change ratios of non-metastatic and metastatic cells. Hence, the detectability of metastatic cells increased. These calculated matrices provided clear and explicit measures to discriminate single cells for their metastatic state on functional nanotextured substrates.

1.2.3. Detection of Cancer Metastasis by Distance Matrix Analysis from Surface Immobilized Tumor Cells in Blood

In metastasis, tumor cells leave primary cancer site, travel through circulatory system, and reach distant organs. Presence of tumor cells in blood can be an effective marker for cancer detection at early stages. In chapter 5, we report aptamer-functionalized nanotextured substrates to capture tumor cells from blood. Anti-EGFR aptamer was used to target overexpressed EGFR on tumor cells. Blood cells and tumor cells were captured separately on the substrates. Captured tumor cells changed their shape over time while blood cells were inactive. Cell shape changes were quantified with distance matrix analysis. Hausdorff distance and Mahalanobis distance analysis showed tumor cells exhibited higher shape change. This translated as higher values in distance profiles of tumor cells compared to blood cells. Tumor cells had 214.9% higher Hausdorff distance

and 274.7% higher Mahalanobis distance than white blood cells (WBCs). Tumor cells displayed characteristic distance profiles in blood and the detection efficiency was 75%. This technique can be an important modality in identifying metastatic tumor cells from blood.

1.2.4. Development of a Non-Invasive Test for Bladder Cancer Detection Based on Cellular Tracking and Distance Matrix Analysis

Detecting bladder cancer from urine sample is a major challenge for clinicians. Current processes conducted to detect bladder cancer before metastasis are mostly invasive. The results also vary widely depending on the technical skill of the pathologists. We report a non-invasive technique to detect bladder cancer cells from urine sample based on morphological change of cells captured on nanotextured anti-EGFR aptamer functionalized substrates in chapter 6. Distance matrices were calculated to quantify cell shape change. Bladder cancer cells had 125.4% higher Hamming distance, 95.9% higher Hausdorff distance and 86.81% higher Mahalanobis distance than healthy urothelial cells. We established distinctive distance profiles for both types of cells. Urine samples from patients known to have bladder cancer were collected and suspended on nanotextured anti-EGFR aptamer modified substrates. The cells which had similar diameter to cancer cells were selected and distance values for these cells were calculated. These distance values were compared with ideal distance values calculated from cell lines and bladder cancer cells could be detected from patient urine sample in this way.

Chapter 2

BACKGROUND AND LITERATURE REVIEW

2.1. Carcinogenesis and Metastasis

Uncontrolled growth of cells is cancer, and spreading of cancer cells to other parts of our body is metastasis. Metastasis starts with direct extension or invasion of cancer cells to surrounding tissues. Cancerous cells then break away from primary tumor and travel through lymphatic or hematogenous system. These cells are circulating tumor cells or CTCs. CTCs in blood contain some cells capable of initiating metastasis growth in other organs. CTCs have been reported to form metastatic deposits recently [1, 2]. They have been found in patients with metastatic cancer [3, 4]. Decreased CTC count has been shown to be associated with higher survival rates in lung, breast, colorectal, and prostate cancer patients [5-8]. Number of CTC is significantly relevant to diagnosis [9] and disease progression [6, 10, 11]. This number is also a good measure of the effectiveness of therapeutic treatments [12, 13].

In this dissertation we have focused on two types of metastatic cancer: breast and bladder cancer. Detecting metastatic breast cancer at an early stage is of great importance for prescribing specific treatments to curtail the spread of disease. For breast cancer, metastasis can reach bone, liver, lungs, and even brain. According to American Cancer Society, in 2016 among the new breast cancer cases 249,000 cases were diagnosed as metastatic while only 61,000 were in situ. The death toll was 40,890 [14]. Only 6-10% of reported breast cancer cases are diagnosed initially as metastatic [15], but eventually 20-30% of all reported breast cancer cases become advanced or metastatic [16]. Breast cancer death rates among women are higher than those for any other cancer, besides

lung cancer [14]. Early detection of metastatic breast cancer can dramatically improve the diagnosis and treatment which in turn can reduce the possibility of occurrence of advanced cancer and improve life expectancy.

Bladder, an extremely important organ of our body is part of the urinary tract in the pelvis and stores urine before excreting it by urination. The flexible and muscular wall of this hollow organ has thin lining made up of urothelial cells. Bladder cancer begins when these cells start to grow and divide uncontrollably and form tumors. Most bladder cancers start in the innermost lining aka urothelium. Cancer may also initiate from the squamous cells or glandular cells. American Cancer Society estimated that 79,030 adults (60,490 men and 18,540 women) would be diagnosed with bladder cancer in the United States and the estimated death would be 16,870 (12,240 men and 4,630 women) in 2017 [17]. Among man, bladder cancer is the fourth most common cancer and the eighth most common cause for death by cancer. Chance for men to develop this cancer during life time is about 1 in 26 [18]. As more cancer cells develop, the disease can grow into the bladder wall and spread to other areas of the body and become more advanced and harder to treat. Metastatic or invasive bladder cancer spreads to nearby lymph nodes, bones, lungs, or liver. About 1 in 3 bladder cancers invade into deeper layers. Sometimes the symptoms of cancer like blood in urine (hematuria), pain during urination, frequent urge to urinate etc. are absent. Often some of the symptoms are confused to be caused by other medical conditions. Hence, finding it early regardless of the symptoms improves the chance of effective treatment and decrease the rate of progression [18]. It is easily evident in the 5-year survival statistics published by American Cancer Society [17]. According to the report, for non-invasive bladder cancer the rate is 96%, for invasive but contained inside

the bladder case it is 70%, for cancer invaded to nearby lymph nodes it is 34% and finally for the completely metastasized cancer it is 5%.

2.2. Cancer Diagnosis

Computed x-ray tomography, magnetic resonance imaging, mammogram, and ultrasound scans are the current diagnostic tools to clinically detect metastasis of breast cancer. The ability of these tools hugely depends on the size and density of the tissue. Mammogram is less likely to find tumors in women younger than 50 years and less than one-tenth of one percent of standard mammograms can lead to cancer diagnosis [14]. Even though these tools can detect tumors in many patients, they are quiet unreliable to detect metastasis as they cannot image metastatic cells traveling inside the body unless the cells form distant micrometastases. At that point the disease is already at the last stage. Currently, researchers are investigating some new imaging tools like positron emission tomography (PET) to acquire molecular and physiological information [19, 20]. FDA has approved PET imaging to specify stage of breast cancer [21]. A group has reported macrophages targeting magnetic nanoparticles to detect millimeter sized lymph node metastases in patients [22]. Another group investigated radiolabeled monoclonal antibodies targeting tumor-specific antigens such as HER2 and carcino-embryonic antigen to image cancer [23]. One of the negative sides of these techniques is they require imaging agents or radiotracers which are often restricted if the patient has any illness, or medical condition like pregnancy, or allergies or is on medication. Sometimes the tracers' slow clearance from the blood causes further complications. Hence, most of these are not FDA approved. As a result, if there is any confusion about a lump, a biopsy is prescribed. Biopsy is followed by histological examination of surgically removed breast

tissue. Cancer stage is determined by the arrangement of cells, shape and size of cells, cell nucleus color when stained, histochemical staining of cancer cells, and immunohistochemical staining of cancer cells with antibody. But in the early stages of metastasis, the number of cells are really small in the tissue and histological examination after biopsy is again not very effective. About 10% of patients who have a mammogram will require further testing. And less than 10% of those will require a biopsy and about 80% of those biopsies will not show cancer [14].

Diagnosis of early stage bladder cancer is a major challenge. The current clinical techniques to detect bladder cancer are urinalysis, urine cytoscopy, cystoscopy, biomarker check and biopsy. In urinalysis, urine is microscopically checked for irregular cellular constituents and blood (gross hematuria or microscopic hematuria) [24]. Blood in urine is the first sign of bladder cancer but can also be caused by benign (non-cancerous) conditions like infections which reduce the potential of this test. For cytology test the doctor uses a microscope to look for cancer cells in urine after cell fixation. Cancerous cells display increased nucleus/cytoplasm (N/C) ratio, hyperchromatism, markedly irregular nuclear borders or prominent nucleoli [25]. But technical preparation, experience and skill of the cytopathologist [26] and intraobserver reproducibility [27, 28] cause variability in result [29-32]. Cytology is not a point of care test and is expensive [33]. Though it is highly specific (>90%) , it is limited by low sensitivity (<50%) [34-37] and unsuitable for low-grade lesions [38]. There are urinary biomarker tests such as UroVysion™ based on FISH which looks for chromosome changes [39-41], BTA tests based on qualitative latex agglutination assay which look for a substance called bladder tumor-associated antigen (BTA) [42], Immunocyt™ based on three monoclonal

antibodies which looks for mucin and carcinoembryonic antigen (CEA), and NMP22 BladderChek® based on quantitative ELISA which looks for a protein called NMP22 [42]. All these testing techniques exhibit a higher sensitivity but a lower specificity [43-48] which also varies test to test. Among the invasive tests, cystoscopy is widely recommended. In this test, a urologist examines the bladder wall with a thin tube directing light. Abnormal areas seen through cystoscopy are biopsied. Cystoscopy is the gold standard investigation. But it can miss small or flat lesions [34], has false-negative rates of 10-40% [49-51] and potential side effects with discomfort and distress of the patient [52]. These tests are yet not full proof because they might find some bladder cancers, but can miss some also. Sometimes the results announce cancer in some healthy people. At this time these tests are mainly used to look for recurrance in bladder cancer patients or in people who already have signs or symptoms of cancer.

2.3. Epidermal Growth Factor Receptor

The most frequently overexpressed receptor tyrosine kinase oncogene is epidermal growth factor receptor (EGFR) which promotes cell migration, invasion proliferation, adhesion, angiogenesis etc. [53-57]. It is present on the cell membrane, and is activated when it binds with different growth factors. In healthy cells, EGFR expression level varies from 40,000 to 100,000 proteins per cell [58]. The expression increases as the cells start to become cancerous. The constant activation of this upregulated receptor leads to uncontrolled cell division which in time turns out to be cancer. Both wild type (WT) and mutated EGFR have been reported to be biomarkers for cancer. Overexpression of WT EGFR is reported to be found on lung cancer and glioblastoma cells while a mutated variant EGFRvIII has also been reported to be present in gliocarcinoma [59]. In non-

metastatic breast cancer cell line MCF-7, EGFR expression is $1.5x10^4$ receptors per cell whereas in metastatic breast cancer cell line MDA-MDB-231, the expression increases to $1.3x10^5$ receptors per cell [60]. Most bladder cancer cells show overexpression of EGFR [61-65]. For bladder cancer cells EGFR expression is around 10^5 sites per cell [66, 67].

2.4. Antibody and Aptamer

Cancer cell detection based on affinity interaction between cell membrane proteins and aptamers is a highly proficient process. Aptamers are single stranded oligonucleic acid or peptide molecules that can selectively bind to specific target molecules. Interaction between membrane protein and aptamer is highly selective and very specific. Aptamers are reported to be better than antibodies in terms of affinity and specificity [68]. They are reported to be highly stable in various salt and ionic conditions. Moreover, aptamers can be immobilized on specific sites very precisely. They can also be reversibly denatured [69]. Aptamers are more hydrophilic than antibodies. These crucial qualities of aptamers have made them preferable to antibodies in detecting cancer cells. In this dissertation, we are using anti-EGFR aptamer to selectively capture metastatic breast and bladder cancer cells based on EGFR overexpression on cell membrane.

2.5. Cancer Cell Detection

To combat cancer at early stages, CTC detection and enumeration in peripheral blood and detection of metastatic cells in biopsy samples have significant clinical importance [70, 71]. CTCs have been evidenced as prognostic markers for breast cancer [72]. To ensure stage specific timely treatment, CTC detection in blood and/or accurate staging of biopsy samples can enhance existing early detection methods. Blood samples are

routinely being extracted from patients' body for any health test and it can be easily used to check for CTCs. But the technical difficulty to detect CTCs in peripheral blood is their rarity [73, 74]. The absolute number varies depending on the progression of the disease, but in most cancer patients it ranges between 1 to 200 cells in 1 ml of blood [13, 74-77].

Current state of the art techniques to isolate CTCs from peripheral blood include immunomagnetic separation, immunocytochemistry detection [6, 78] and reverse transcriptase-polymerase chain reaction [79-82]. Among other techniques, direct visualization assay [75], fluorescence activated cell sorter [83], array scanning technology cytometer based on fiber optics [77], anti-EpCAM coated microstructures [84] etc. have also been reported. Most of these techniques are tedious and complicated with long processing time and expensive equipments [84, 85]. These are also limited by cell purity and yield [86].

2.6. Nanostructured Substrates

Nanotextured substrates are the emerging biosensing platforms to capture or isolate cancer cells. Nanotexture increases the effective surface area of substrates and augments sensitivity; but the tradeoff is specificity. This problem is overcome by introducing specific antibodies and aptamers. The idea of introducing nanotexture in device design comes from nature. Micro or nanoscale structures are vastly seen in plants, insects, and even in human tissues. The vascular endothelial basement membranes in human body have 3D nanoscale topography. This kind of structure influences cellular functions significantly [87]. Cancer cells anchor to basement membranes using cell adhesion molecules and invade the barrier [88]. Nanoscale structures provide higher interactions with biomolecules, which is a primary requirement for any sensing technique.

The sensing devices often use defined nanotopography for cell capture [84]. To study cell morphology, adhesion, and migration, Fischer et al. used micro and nanoscaled array of silicon pillars [89]. To separate T lymphocyte, 100-200 nm sized silicon nanowires functionalized with streptavidin were used. Resulting capture efficiency was 88% [90]. We previously reported synthesis of a biocompatible scaffold from nanotextured chicken eggshell [91]. Such nanotextured scaffolds can remarkably increase the density of some cells [92, 93].

Chapter 3

DISCRIMINATION OF METASTATIC BREAST CANCER CELLS FROM INDOLENT CELLS ON APTAMER FUNCTIONALIZED SURFACE WITH IMAGING BASED CONTOUR FOLLOWING TECHNIQUES

3.1. Introduction

To effectively detect metastatic breast cancer cells, here we report a simple post-biopsy imaging technique on aptamer functionalized substrates. This is a label-free, single cell analysis technique where each and every cell can be examined for metastatic behavior. Examination of each and every cell presents high probability of detecting metastatic cells even though the number of these cells may be very small in patient sample.

In this chapter, the capture and detection of metastatic breast cancer cells MDA-MDB-231 is reported based on their unique morphological characteristic on anti-EGFR aptamer immobilized glass substrates. Metastatic breast cancer cells changed their morphology with time when captured on anti-EGFR aptamer functionalized glass substrates. Non-metastatic MCF-7 cells captured on aptamer-modified substrates did not show this behavior. Based on this distinguishable trait of metastatic and non-metastatic cells on functionalized glass substrates, we established a detection technique. We used distance matrix analysis to compute shape change of cells from optical image. The technique was tested on a cell mixture of metastatic and non-metastatic cells mimicking a biopsy sample. In biopsy we extract different types of cells including metastatic ones. It is hard to detect metastatic cells from non-metastatic cells using current technology. The technique

presented here can successfully detect metastatic cells from this mixture based on their morphological alteration on aptamer grafted substrates.

We have reported efficient capture of human glioblastoma cells from astrocytes on aptamer grafted substrates previously [94, 95]. Cell capture technique is very popular for its selectivity and the efficiency of our reported technique for glioblastoma cell capture was higher than astrocytes. But in the captured cell population, distinction of cells was not possible. We later showed that there was morphological non-uniformity between glioblastoma and astrocyte cells on aptamer modified substrates [95]. Here, we show a precise distance matrix based cell shape analysis technique to differentiate between metastatic and non-metastatic breast cancer cells on aptamer modified substrate.

3.2. Materials and Methods

All chemicals used in the experiments were obtained from Sigma-Aldrich (St. Louis, Missouri, USA), unless mentioned otherwise.

3.2.1. Substrate Preparation

Fisher brand microscope slides were used as substrates. The glass slides were cut into 5 mm x 5 mm pieces and cleaned with Piranha solution (H_2SO_4:H_2O_2::3:1) for 10 minutes to remove any contaminant and create –OH groups. The substrates were subsequently washed with deionized (DI) water and dried in N_2 flow. To remove any moisture, a baking step at 195 °C for 10 minutes was done. To create amine groups on the surface, the substrates were immersed into 200 µl of 2% (3-Aminopropyl)triethoxysilane (APTES) for 30 minutes. After a thorough rinse with isopropyl alcohol (IPA) and DI water, the substrates were dehydrated again at 150 °C for 30 minutes. A solution of 9 ml dimethyl

sulfoxide (DMSO), 1 ml pyridine and 0.002 gm *p*-Phenylene diisothiocyanate (PDITC) was prepared to immerse the substrates for 5 hours at 45 °C. After another washing with IPA and diethylpyrocarbonate (DEPC)-treated water, unreacted PDITC end groups were capped to prevent any nonspecific adsorption. To do that, the substrates were immersed in 150 mmol/l N,N-Diisopropylethylamine (DIPEA) in dimethylformamide (DMF) and 50 mmol/l 6-amino-1-hexanol for 5 hours. PDITC created a diisothiocyanate layer on the substrates, one end of which attached to the glass substrate-tethered APTES and the other end could bind to amine-bearing capture molecules. We used amine modified DNA as capture molecules. The amine modified capture DNA had the sequence: 5′-amine-CTGGTCATGGCGGGCATTTAATTC-3′ and was diluted with DMSO [94]. Then each of the glass substrates was loaded with 20 µl of 5 µM capture DNA and was incubated for 18 hours at 45 °C in a humid chamber. This capture DNA would later bind with the aptamers.

3.2.2. Aptamer Preparation and Substrate Functionalization

The sequence for anti-EGFR aptamer was: 5′-GGC GCU CCG ACC UUA GUC UCU GUG CCG CUA UAA UGC ACG GAU UUA AUC GCC GUA GAA AAG CAU GUC AAA GCC GGA ACC GUG UAG CAC AGC AGA GAA UUA AAU GCC CGC CAU GAC CAG-3′ [94]. The underlined part is the complementary chain which could bind with the capture DNA. As a negative control, to show lack of non-specific binding, a mutant aptamer sequence was used (5′-GGC GCU CCG ACC UUA GUC UCU GUU CCC ACA UCA UGC ACA AGG ACA AUU CUG UGC AUC CAA GGA GUU CUC GGA ACC GUG UAG CAC AGC AGA GAA UUA AAU GCC CGC CAU GAC CAG-3′) [94]. The anti-EGFR and mutant aptamers were diluted with DEPC-treated water and mixed with hybridization buffer

(5:1::RNA:hybridization buffer). After 18 hour incubation period, the DNA incubated substrates were washed with IPA and DEPC water. A volume of 25 µl aptamer was placed on a substrate. Half the substrates were incubated with anti-EGFR aptamer while the other half were incubated with mutant aptamer. All the substrates were incubated at 37 °C for 1 hour in an incubation chamber. The chamber was previously washed with RNase-free and DEPC treated DI water. After incubation, substrates were washed with 1X phosphate buffered saline (PBS), (pH 7.5) solution and used immediately.

3.2.3. Target Cell Preparation

Two types of breast cancer cells were used. The metastatic cell line was MDA-MDB-231 and the non-metastatic cell line was MCF-7. They were obtained from the University of Texas Southwestern Medical Center (Dallas, TX). The cells were cultured in Dulbecco's modified Eagle's medium (DMEM/F-12; Cellgro, Corning, Manassas, Virginia, USA) with 10% heat inactivated fetal bovine serum. L-glutamine (Invitrogen, Carlsbad, California, USA) and Gentamycin were also added to the medium. A sterile humidified culture environment was maintained with 95% air and 5% CO_2 at 37 °C. In all experiments, the cells were first centrifuged to remove supernatants and then diluted with sterilized and warm 1× PBS solution. The prepared cells were immediately used.

3.2.4. Cell Mixture Preparation

Two sets of experiments were conducted with metastatic and non-metastatic cells. In the first set of experiments, both types of cell were captured on anti-EGFR aptamer and mutant aptamer modified substrates separately. Cells were observed and images were taken. The distinctive morphological characteristics of metastatic and non-metastatic cells were established and quantified from this experiment.

In the second set of experiments, a mixture of metastatic and non-metastatic cells was used. The metastatic cells were tagged with 5-chloromethylfluorescein diacetate (CMFDA; Thermo Fisher Scientific, Carlsbad, California, USA). This fluorescent dye was used for tracking cell motility. The emission spectra were 492/517 nm. CMFDA (0.2 µl) was mixed in 1 ml of the medium. The tagged metastatic and untagged non-metastatic cells were mixed in 1:1 ratio. The purpose of this experiment was to track morphology change of the cells temporally and detect metastatic cells from the mixture based on previously established quantitative metrics.

3.2.5. Cell Suspension and Image Capture

In the first set of experiments, the prepared cells were suspended in 1x PBS solution. These were then loaded on the 5 mm x 5 mm functionalized glass substrates. Typically, a volume of 30 µl cell suspension was used to cover each substrate. The density of non-metastatic cell suspension was 200,000 cells/ml and for metastatic cell suspension was 100,000 cells/ml. Usually 3 or 4 minutes were given to let the cells settle down on the functionalized substrates. After settling down the average concentration of cells on functionalized glass substrates was ~120 cells per mm^2 for metastatic cells and ~240 cells per mm^2 for non-metastatic cells. To inspect cell attachment on the substrates and their behavior over the time, an optical microscope was used. Three samples from each of the four groups of cell-RNA pairs were analyzed: metastatic cells captured on anti-EGFR aptamer functionalized substrates, metastatic cells captured on mutant aptamer functionalized substrates, non-metastatic cells captured on anti-EGFR aptamer functionalized substrates, and non-metastatic cells captured on mutant aptamer functionalized substrates. The cells on all 12 substrates were imaged. Over the next 30

minutes, images were taken 30 seconds apart using a Leica DM series optical microscope with DFC295 color camera at 20X magnification.

In the second set of experiments, CMFDA tagged metastatic and untagged non-metastatic cell pellets were mixed inside 1X PBS solution in 1:1 ratio and suspended on anti-EGFR aptamer modified substrates. Then the cells were imaged with Zeiss fluorescence microscope (Axioplan 2 LSM) with AxioCamMR3 camera.

3.2.6. Image Analysis

The captured images were analyzed with custom written code in MATLAB. From the images, each cell was cropped and arranged sequentially with respect to time. A batch of images was generated for each cell showing its shape change with time. These images were in RGB format. They were processed via edge detector code which generated batches of binary images. All the binary images were processed in a way that the center of the cell was always at the same position. This precaution was taken due to the fact that some cells moved a little bit with time while still attached to the surface. Each of these batches of binary images was processed using our code to quantify their shape change.

3.2.7. Cell Contour Detection

The computational procedure for cellular edge detection was based on level set algorithm. The RGB images were processed with Wiener filter for noise removal. Wiener filter is a low pass filter which removes noise by adapting to pixel wise statistical estimation of the local neighborhood. The adaptive nature of Wiener filter worked better than linear filters due to its capability to preserve edges. The images were further smoothed by Gaussian filter. Cellular edge was the place of rapid change in the intensity profile of the image.

Therefore, cellular edge corresponded to the extremas of the derivatives of image intensity. Gradients of the images were calculated which indicated the places with most rapid intensity change i.e. cellular edge. The strength of the edge is calculated by the magnitude of the gradient. From this magnitude an edge indicator function is calculated with the following formula:

$$Edge\ indicator\ function = \frac{1}{1+Magnitude\ of\ gradient^2}.$$

The level set method is a dynamic process which tracks the motion of an interface [96]. The interface is called zero level set and in our case it was the image boundary. When the image boundary aka zero level set started to move inwards and towards the cellular edge, we got an initial value partial differential equation. In solving this equation Neumann boundary condition was used. Neumann boundary consisted of the derivatives of the image intensity.

The tracked boundary from the level set method was compared with the edge indicator function over and over until matched. In this way we segmented the cells from non-cell background by detecting the cell contour.

3.2.8. Shape Similarity Calculation

The segmented cells were converted to binary where the cell body was black and the background was white. To quantify the cell shape change, we employed a shape similarity matching technique. The cells were tracked over time with an optical microscope and images were taken for 30 minutes. These images were converted to binary formats by contour detection. The binary data was matched from image to image. The binary data

had a 1 value where cell body was present and a 0 meant absence of cell body. A 2x2 contingency table was generated for each pixel to match two consecutive images. The 4 conditions that dictated the table were: presence of cell body in both images, ‘a’; presence of cell body in first image and absence in second image, ‘b’; absence of cell body in first image and presence in second image, ‘c’; absence of cell body in both images, ‘d’. For a pixel, only 1 of the 4 conditions had to be true. A value of 1 was assigned for the true condition and 0 for false. A similarity coefficient, Sokal-Sneath coefficient [20], was calculated from this table. The mathematical formula is:

$$Sokal\ Sneath\ coeffcient = \frac{a}{a + 2(b + c)}$$

Mutually absent attribute or ‘d’ was not necessary for similarity calculation, according to Sokal-Sneath [20]. When two binary shapes were similar, ‘a’ was very large; as well as the similarity coefficient. If a cell did not change shape significantly, it remained similar to its previous form and would generate a high similarity coefficient. Continuous morphological change of a cell thus depicted lower values of coefficient.

3.2.9. Distance Matrix Calculation

Distance matrix analysis is a more rigorous method for comparing cell shape. It is a statistical method of pattern recognition, where each pattern is described in terms of features. In our case, we calculated two features: Hausdorff distance and Mahalanobis distance. Features were computed in a way that for different patterns there were non-overlapping feature spaces. We calculated and established Hausdorff distance profile and Mahalanobis distance profile for metastatic and non-metastatic cells. These distance

profiles clustered in clearly recognizable manners to distinguish metastatic and non-metastatic cells based on a decision boundary.

The first distance matrix, called Hausdorff distance, calculated the resemblance between cell contours in two consecutive images [97]. If A and B are the sets of points on the cell contour in two consecutive images, the distance is:

$$H(A,B) = \max\big(h(A,B), h(B,A)\big)$$

where, $$h(A,B) = \max_{a\epsilon A} \min_{b\epsilon B} |a-b|$$

Hausdorff distance minimizes positional errors with nominal and fast calculations. The distance between two closed sets is zero if and only if both sets are identical. That means, if the cells are not showing any morphological change, the Hausdorff distance will be ideally zero or practically a small number. If a cell is changing shape, distance will be a larger number.

Another distance matrix, called Mahalanobis distance, measures the numbers of standard deviations the cell periphery is away from mean cell boundary [98]. It is calculated from the formula:

$$D^2 = (x-m)^T C^{-1} (x-m)$$

where, D = Mahalanobis distance, m = Vector of mean values from initial cell boundary, x = Vector of changing cell boundary, C^{-1} = Inverse covariance matrix of initial cell boundary, and T = Transpose vector.

3.3. Results and Discussion

3.3.1. Dynamic Tracking of Morphological Characteristics of Cells

The metastatic and non-metastatic cells were captured separately on anti-EGFR aptamer and mutant aptamer modified substrates. The captured cells were tracked for 30 minutes. Over this time, the metastatic cells changed their shapes on anti-EGFR aptamer modified substrates by creating protrusions form cell membranes. The non-metastatic cells captured on anti-EGFR aptamer functionalized substrates did not show such changes in shapes. Both types of cells captured on mutant aptamer functionalized substrates did not show any morphological changes. It was unique for metastatic breast cancer cells captured with anti-EGFR aptamer to show distinctive morphological behaviors. This feature was used to identify metastatic breast cancer cells from non-metastatic ones.

Metastatic and non-metastatic cells captured with mutant aptamer showed the same behavior (no shape change) as non-metastatic cells captured with anti-EGFR aptamer. For simplicity in presentation, results from cell morphology on mutant aptamer functionalized glass substrates are not shown in the data analysis. Results for non-metastatic cells captured with anti-EGFR aptamer are good representations of metastatic and non-metastatic cells captured on mutant aptamer functionalized glass substrates.

The temporal optical micrographs in Fig. 3-1 show the morphological change of cells with time. The metastatic breast cancer cells showed morphological changes when captured with anti-EGFR aptamer (Fig. 3-1(a)). Micrographs of 5 different metastatic cells exhibited this behavior over time. Non-metastatic cells captured with either anti-EGFR aptamer or mutant aptamer and metastatic cells captured with mutant aptamer did not show such behavior (Fig. 3-1(b)).

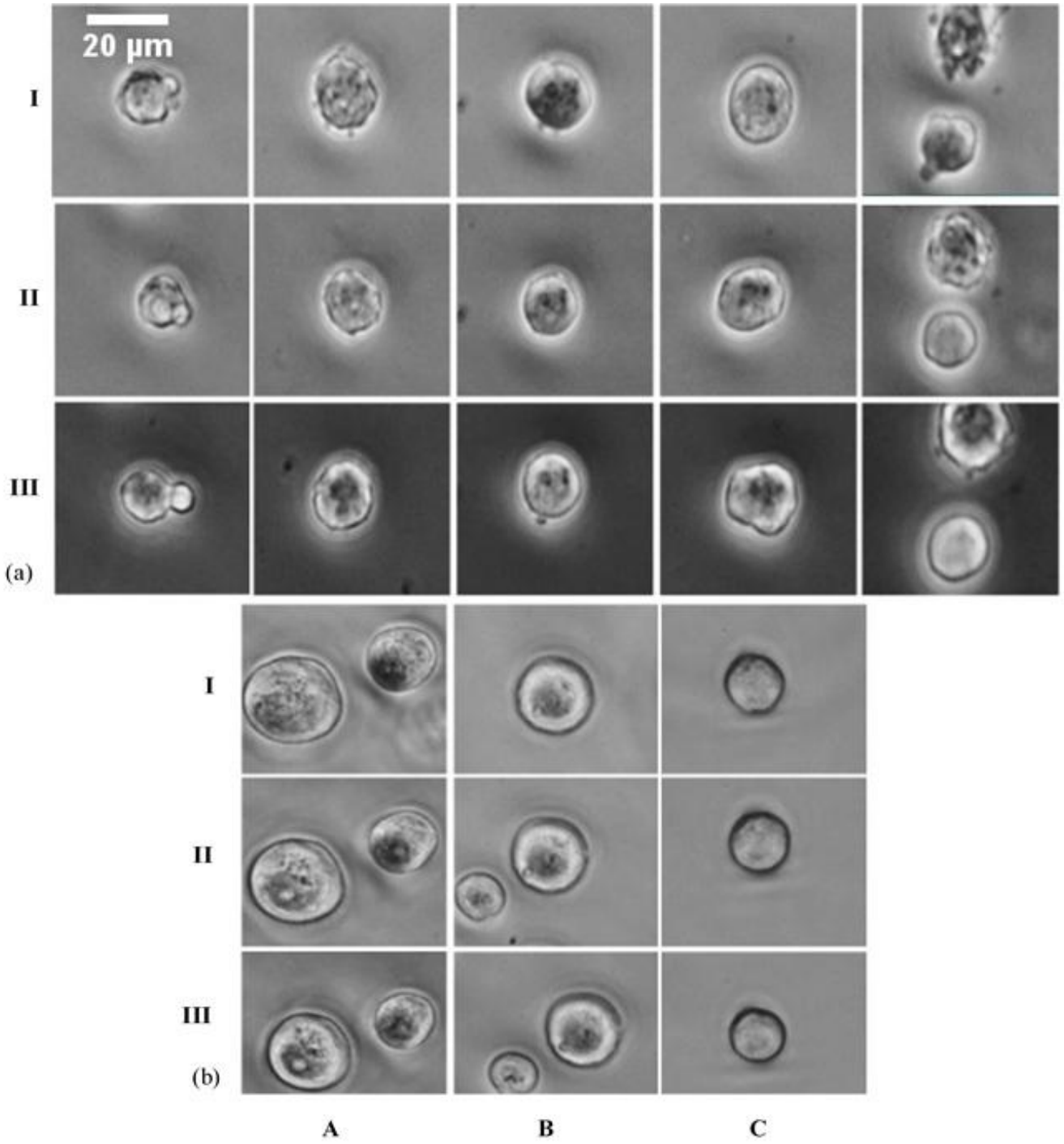

Figure 0-1: (a) Metastatic cells captured with anti-EGFR aptamer. Micrographs of 5 different cells after (I) 2 minutes, (II) 9 minutes, (III) 17 minutes of capture. Each cell shows change in contour with respect to time; (b) (A) Non-metastatic cell captured by anti-EGFR aptamer, (B) Non-metastatic cell captured by mutant aptamer, (C) Metastatic cell captured by mutant aptamer. Micrographs taken after (I) 2 minutes, (II) 9 minutes, and (III) 17 minutes of capture. Non-metastatic cells do not show any morphological change over time.

The morphological changes of metastatic cells on anti-EGFR aptamer modified substrates can be explained by the expression of EGFR on their cell membrane. Metastatic breast cancer cells have 10 times more EGFR than their non-metastatic counterparts [60]. EGFR detects specific signals for cell movement, proliferation and migration [99, 100]. Metastatic breast cancer cells, having higher density of EGFR, created more receptor-aptamer bonds than non-metastatic cells. In these cells, more activated EGFRs generated cascades of intracellular signals. It is known that intracellular signaling stimulated by EGFR results in continuous restructuring of actin filaments [101]. Overexpression of EGFR thus triggered dynamic rearrangement of cytoskeleton structure of metastatic cells on anti-EGFR aptamer functionalized substrates.

3.3.2. Shape Similarity Matching

In Fig. 3-2(a), average Sokal-Sneath coefficient is presented for metastatic and non-metastatic cells with time. It is a similarity coefficient and lower value of coefficient meant cell shape was changing prominently with time. Average for non-metastatic cells was more than 0.9 a.u. during the whole 30 minute period, confirming a high similarity. For metastatic cells, the average was much lower for first 10 minutes. Later, it increased but still stayed below 0.9 a.u. The propensity of changing morphology for metastatic cells was observed to gradually decrease with time. It can be inferred that after around 20 minutes, the cytoskeleton rearrangement of metastatic cells was finally stable. In Fig. 3-2(b), the contrast comparison is shown with respect to time. While for non-metastatic cells the average coefficient is almost the same (~0.9 a.u.) over time, for metastatic cells it changed from 0.77 a.u. (at 4 min) to 0.84 a.u. (at 28 min). The average coefficients for metastatic cells are significantly different than that for the non-metastatic cells in both time

points (p-value < 0.01). For better diagnostics, the contrast between metastatic and non-metastatic cells is preferable to be strong. And the early coefficient values give a better diagnostic.

Lower similarity resulting from more inclination to change morphology of metastatic cells on anti-EGFR aptamer functionalized substrates confirmed the fact that the cytoskeleton structure of these cells were more flexible than non-invasive cancer cells [26-28]. The actin filaments of the cytoskeleton have been reported to be very agile in metastatic cells [29, 30].

Over the imaging period, it was observed that the cells spread out on the substrate. Hence, their size changed in the 2D images. For coefficient analysis, where we took every pixel change into account, this event laid an undesirable influence and decreased the sensitivity of this metric. We calculated distance matrices to avoid this problem. Distance matrix analysis was done only on cell contours. Though cell contours also changed due to spreading out, the change was subtler than cell area change. Although coefficient analysis was burdened with cell spreading phenomenon, but it still presented a quick and simple measure to indicate dynamic morphology of metastatic cells.

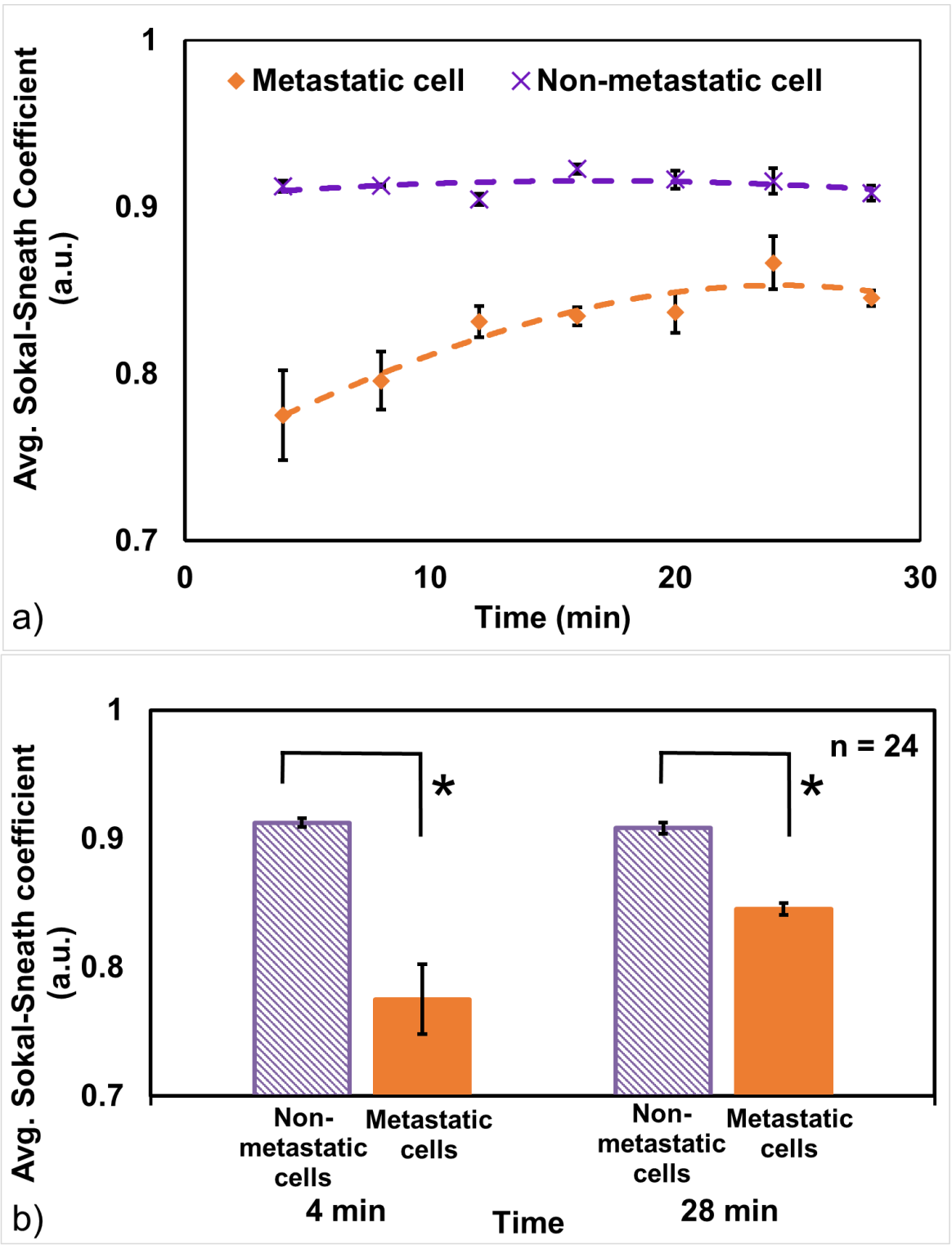

Figure 0-2: (a) Average Sokal-Sneath coefficient of metastatic and non-metastatic cells with time. The trend shows metastatic cells have lower coefficient value, which means cell shape was changing with time. Non-metastatic cells are uniformly showing higher similarity with a coefficient value closer to 1, where 1 means exactly same shape. (b) Contrast comparison between metastatic and non-metastatic cells with time based on Sokal-Sneath coefficient (*, *p*-value < 0.01).

3.3.3. Hausdorff Distance Profile for Metastatic and Non-metastatic Cells

In Fig. 3-3(a), the average Hausdorff distance for metastatic and non-metastatic cells are shown with time. Higher Hausdorff distance meant higher cell shape change. The non-metastatic cells showed a low and uniform distance over 30 minutes. Due to constant morphological change of metastatic cells, their distance values were higher. From this analysis, it was again evident that the shape changing tendency of metastatic cells subsided after around 20 minutes. When activated EGFR on cell membrane triggered intracellular signaling pathways, actin-modifying proteins were released from the cell membrane which reorganized actin cytoskeleton [102]. Filopodia/lamellipodia extension and retraction from cell membrane was controlled by actin cytoskeleton. Presence or absence of suitable binding sites on the substrates stabilized the extension or retraction of filopodia/lamillipodia [103, 104]. Stable binding between surface-bound anti-EGFR aptamer and cell membrane EGFR ultimately suppressed cell morphological change after 20 minutes. The total distance value after 30 minutes consists of the high-contrast early values and low contrast late values. It is true that we could only take the high-contrast early values for discrimination. But from our results we concluded that inclusion of the low-contrast late values augmented the metrics and enhanced the difference between metastatic and non-metastatic cells. Average Hausdorfff distance after 30 minutes is plotted for both types of cell in Fig. 3-3(b). The average was 1.5 a.u. (SD=0.4 a.u.) for non-metastatic cells and 2.8 a.u. (SD=0.7 a.u.) for metastatic cells. Two-tailed *t*-test confirmed that the averages were statistically significant (p-value < 0.05).

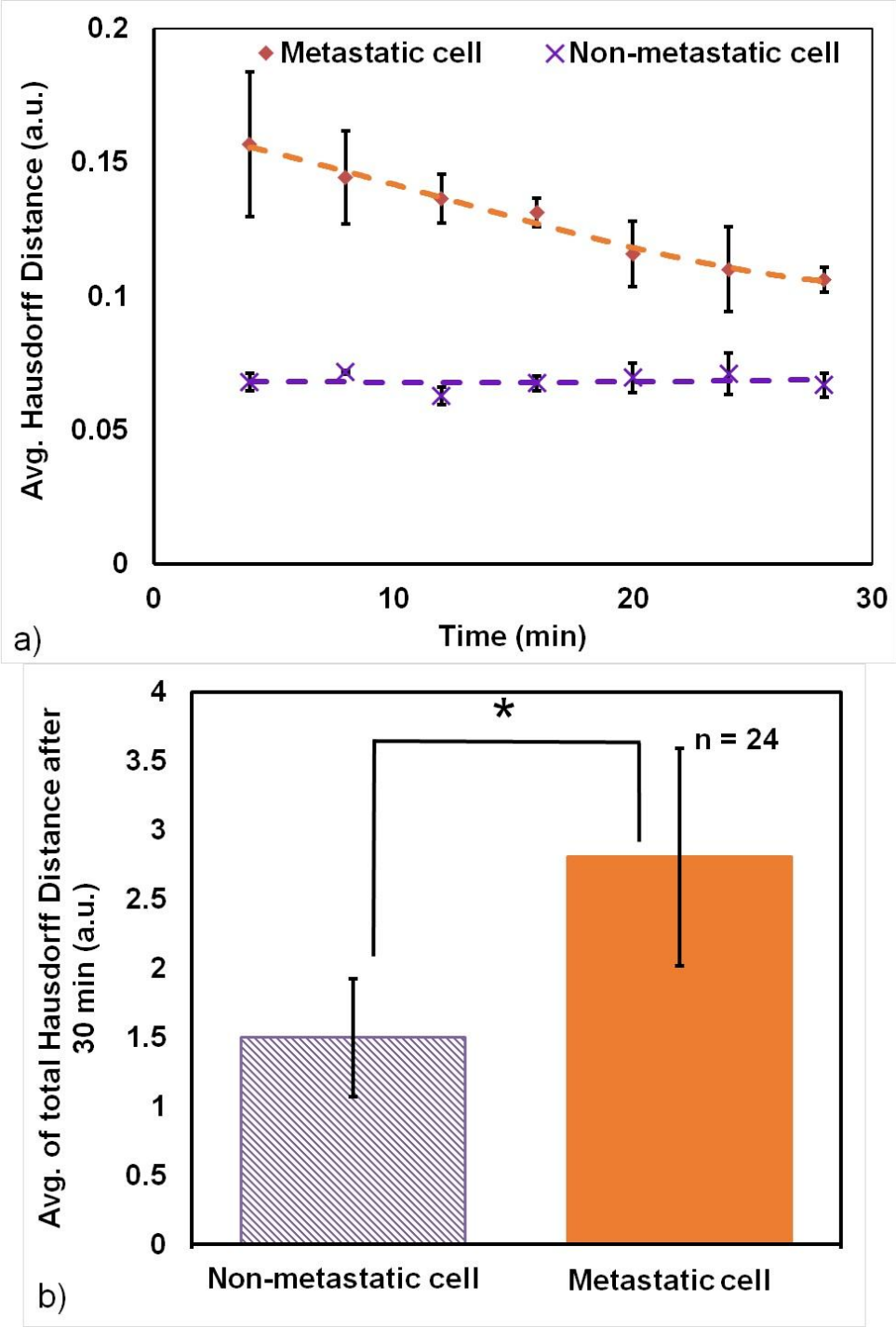

Figure 0-3: (a) Average Hausdorff distance of metastatic and non-metastatic cells with time; (b) Average of total Hausdorff distance of both type of cells after 30 minutes. Two-tailed *t*-test showed *,*p*-value < 0.05.

Metastatic cells have the unique ability to move into tissues surrounding the primary cancer site. This aberrant behavior is caused by genetic mutations. One such mutation happens in the EGFR family of genes [105]. Genetic alteration of EGFR gene is reported to result in upregulation of EGFR on cell membrane of metastatic cells [106]. We employed this fact to capture metastatic cells with anti-EGFR aptamers. Upregulated growth factor driven signaling boosted cell motility in metastatic cells.

3.3.4. Mahalanobis Distance Profile for Metastatic and Non-metastatic Cells

Larger Mahalanobis distance value means larger change in the cell boundary. In Fig. 3-4(a), this distance is plotted with respect to time. The metastatic cells showed higher dissimilarity than non-metastatic ones. The non-metastatic cells showed a more uniform trend than metastatic cells. Average Mahalanobis distance after 30 minutes is shown in Fig. 3-4(b). The averages are 0.7 a.u. (SD=0.27 a.u.) and 0.31 a.u. (SD=0.08 a.u.) for metastatic and non-metastatic cells respectively. Two-tailed *t*-test showed that the distance values for metastatic cells were significantly different from that of non-metastatic cells (p-value < 0.05).

Hausdorff distance analysis is very precise and includes very small positional change of cell contour in calculation. Cells are alive entities and it is usual for any cell to show small shape change over time. As a result, Hausdorff distance analysis is sometimes overloaded and the detection contrast between metastatic and non-metastatic cells decreases. On the other hand, Mahalanobis distance analysis is based on mean boundary of cell and its covariance matrix with new boundary. Hence, Mahalanobis distance sometimes misses subtle change in shape that is expected to be taken into account and over-amplifies the contrast between metastatic and non-metastatic cells. We

combined these two features to counterbalance the imprecise calculations and came up with combined distance profile for metastatic and non-metastatic cells.

We observed that similarity coefficient took cell area into account. Even a very small change of cell shape was amplified in the calculated similarity coefficient and produced huge variability in average values. Whereas distance matrices circumvented the cell spreading effect to some extent. Both type of calculations can thus give us insight into the cell activity over time.

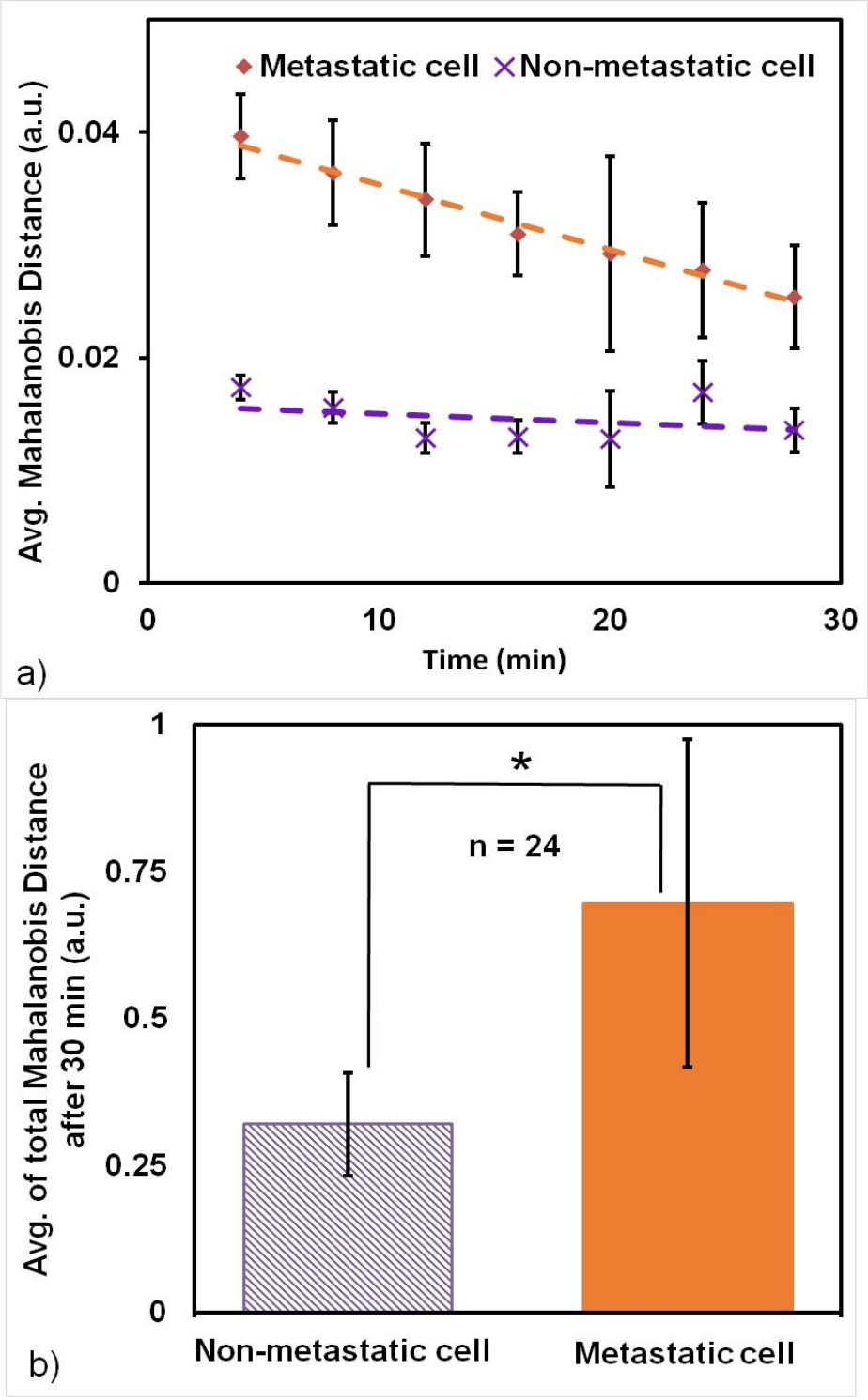

Figure 0-4: (a) Average Mahalanobis distance for metastatic and non-metastatic cells with time; (b) Average of total Mahalanobis distance of both type of cells after 30 minutes. Two-tailed *t*-test showed *,*p*-value < 0.05.

3.3.5. Detection of Cells from Cell Mixture Based on Distance Profile

From distance matrix analysis we could successfully differentiate metastatic cells from non-metastatic ones from their morphological behavior on anti-EGFR aptamer modified substrates. For the purpose of clinical applications to detect metastatic cells, we demonstrated our technique in a cell mixture. Metastatic and non-metastatic cells were mixed in 1:1 ratio. The anti-EGFR aptamer modified substrates were incubated with the cell mixture and imaged for 30 minutes. Metastatic cells, tagged with CMFDA, were confirmed from fluorescence imaging. Fig. 3-5(a-b) show the cell mixture under optical and fluorescent microscopes.

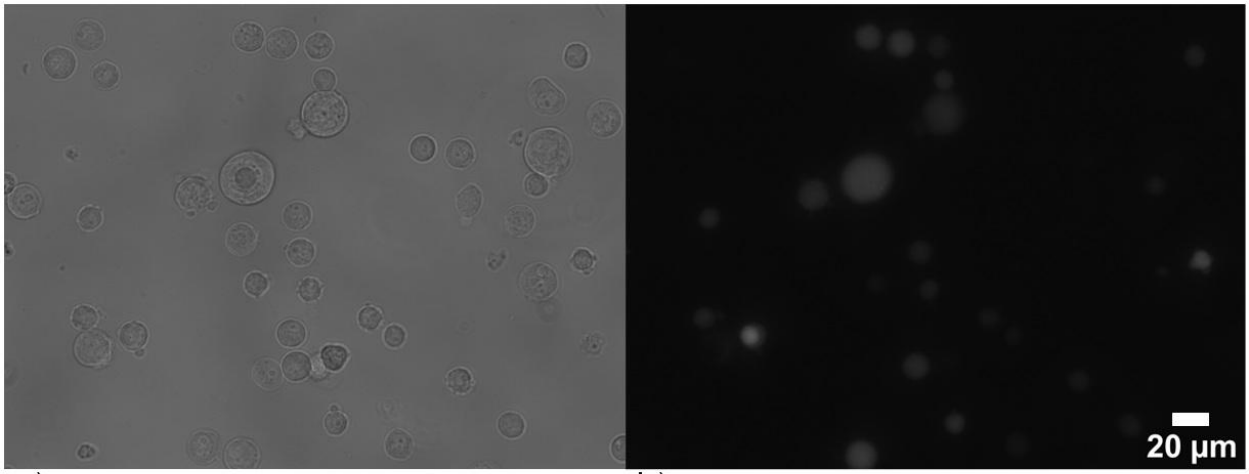

Figure 0-5: (a) Optical and (b) fluorescent image of metastatic and non-metastatic cell mixture at 1:1 ratio. Metastatic cells were tagged with CMFDA. Fluorescent imaging was used to backtrack the identity of cells.

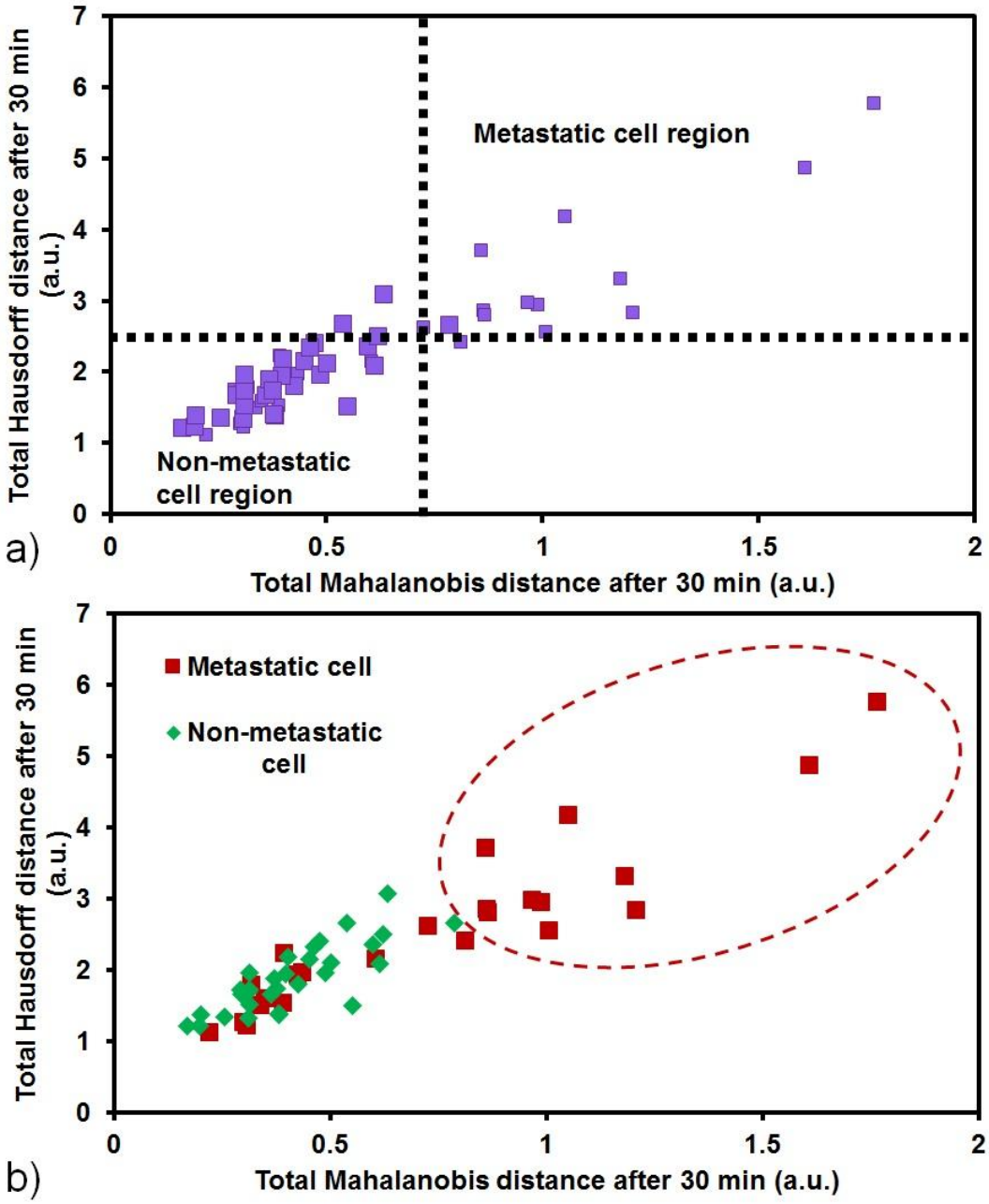

Figure 0-6: (a) Cells from metastatic and non-metastatic cell mixture captured on aptamer modified substrate are plotted according to their distance profile. Metastatic and non-metastatic cell regions are established based on previous distance matrix analysis. (b) Metastatic and non-metastatic cells are plotted from fluorescent image. The red dotted line is previously established metastatic cell region containing 52% of the metastatic cells from the cell mixture.

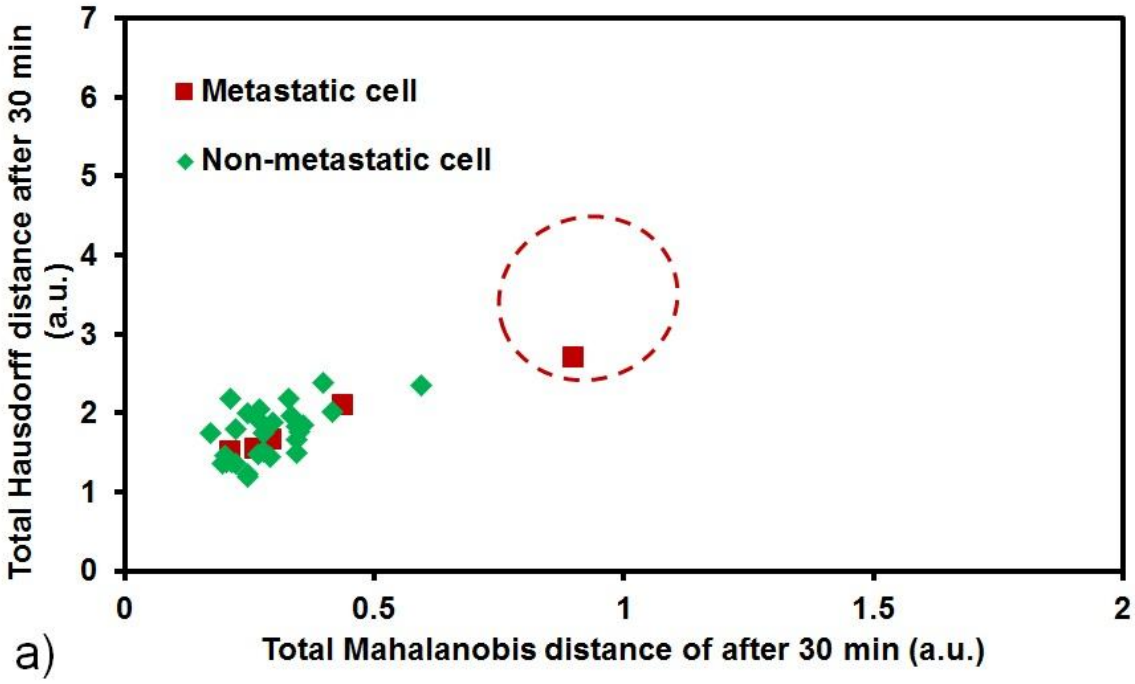

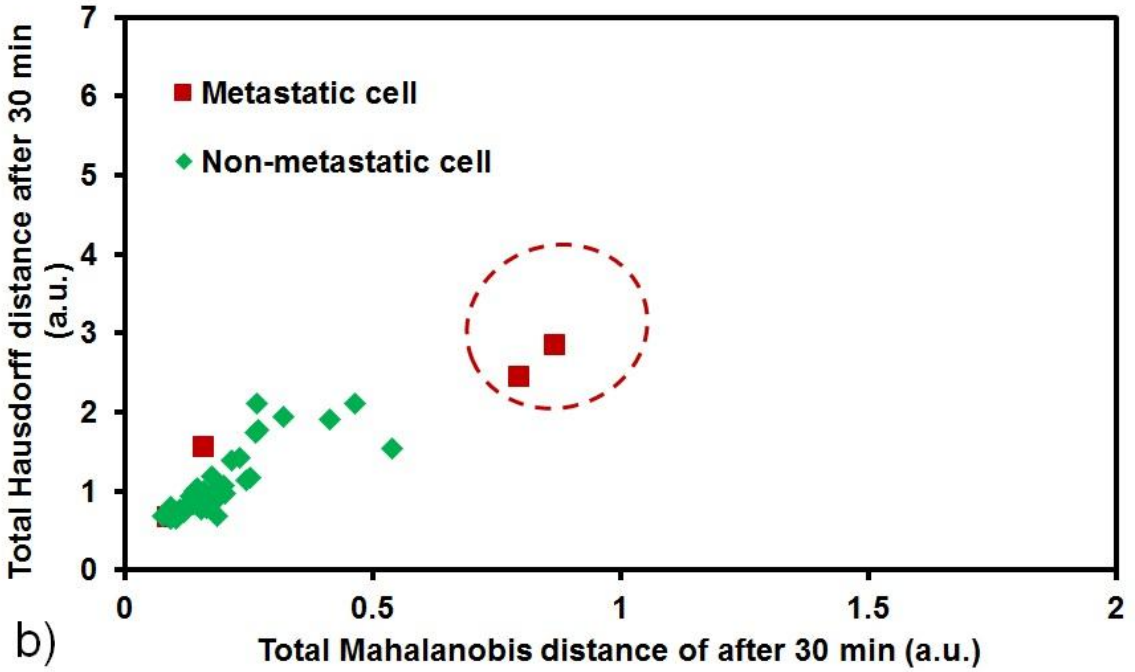

Figure 0-7: (a) Mixture of metastatic and non-metastatic cells::1:6; 1 out of 5 metastatic cell could be detected (circled within red dotted line) (b) Mixture of metastatic and non-metastatic cells::1:10; 2 out of 4 metastatic cells could be detected (circled within red dotted line).

Cell images on anti-EGFR aptamer functionalized substrates were converted into binary format and distance matrix data were accumulated. In Fig. 3-6(a) the captured cells from the mixture are plotted with respect to their Hausdorff and Mahalanobis distances. We took these two parameters because both are distances, and their combination gave the analysis flexibility with precision. A 2D distance profile is simple, sensitive and more robust as advantage of one parameter balances the disadvantage of the other. It was demonstrated that metastatic cells had average Hausdorff distance of 2.8 a.u. (SD=0.7 a.u.) from Fig. 3-3(b) and average Mahalanobis distance of 0.7 a.u. (SD=0.27 a.u.) from Fig. 3-4(b). Combining these features we hypothesized that we can expect metastatic cell population around and beyond these values. In Fig. 3-6(a), we established regions where we expected metastatic and non-metastatic cells to be present. We did find some cells inside the metastatic region. We overlaid the fluorescent image on the optical image to confirm cell identification. Fig. 3-6(b) shows results from the fluorescent image and in our established metastatic region all cells were metastatic (inside red dotted circle). We could thus successfully detect 52% metastatic cells from the mixture. Two more experimental results are shown in Fig. 3-7(a-b).

Cell motility on anti-EGFR aptamer modified substrates can be a novel biomarker for detection of metastatic cells from other cells. Non-metastatic cells closely resemble metastatic cells in size and shape. In biopsy samples, where both invasive and benign cancer cells are present, it is extremely important but difficult to differentiate between these two. Our results suggest that implementation of shape similarity analysis method with anti-EGFR aptamer functionalized capture substrates can be an exciting new strategy for detecting metastatic breast cancer cells in a breast tissue environment. The

technique also eliminates the inadequacy of single cell addressing that exists in current clinical imaging systems. Cell staining often impedes normal cellular function which can be unfavorable for cancer cell identification. Our technique is label-free and selective. Our work is based on ‘immobilization’ of anti-EGFR aptamers on surface for capturing cancer cells [94]. Capture of cancer cells is necessary for further protein or nucleotide study. The captured cells can be later collected by washing off from the surface for these studies. It is difficult to maximize isolation of metastatic cancer cells based on EGFR expression as the expression is just 10 fold from non-metastatic to metastatic cells. Our work has introduced a ‘detection stage’ in between the ‘capture’ and ‘collection’ stage to confirm detection and capture of metastatic cells and maximize their collection.

From our current and previous work [94] and other studies on cell motility due to EGFR binding [102-104], we confirmed that the cause of the reported behavior of metastatic cells is high EGFR expression. We can infer that for other cell lines this should also hold true. But the sensitivity of the detection will certainly depend on the absolute expression of EGFR and the effectiveness of the calculated metric. We also expect metastatic cancer cells in real patient sample will show same kind of behavior as it is based on EGFR overexpression.

3.4. Conclusions

We have presented a simple but elegant way of differentiating metastatic and non-metastatic breast cancer cells. Based on well-defined characteristics, our shape matching technique could differentiate and detect metastatic cells from cell mixture that mimicked composition of breast cancer tissue. This capture procedure and morphological feature

calculation can be used as a simple platform to develop a cost effective and efficient point of care device to detect metastatic breast cancer at an early stage.

Chapter 4

FUNCTIONALIZATION OF NANOTEXTURED SUBSTRATES FOR ENHANCED IDENTIFICATION OF METASTATIC BREAST CANCER CELLS

4.1. Introduction

Previously, we have fabricated random nanotopography on substrates that could selectively capture 93% of cancer cells when functionalized with aptamer [56, 57, 107, 108]. Morphological change of brain cancer cells on these substrates have been reported by our group also [94, 95]. Our platform was simple and easy to fabricate. Use of aptamers provided higher selectivity and specificity against epidermal growth factor receptor (EGFR) of cell membrane.

Using the differential expression of EGFR, we report measurements of differential morphology of metastatic and non-metastatic breast cancer cells on anti-EGFR aptamer coated plane and nanotextured substrates. This modality can be used to define metastatic grade of a given sample whether the cells come from biopsy sample or collected from blood (e.g. circulating tumor cells). In this work, we introduced nanotexture on our platform. Nanotexturing modulated and amplified the activity of captured cancer cells. The effect was much more pronounced for metastatic breast cancer cells. These cells changed their shapes rapidly on nanotextured substrates distinguishing them from non-metastatic cells. A number of quantitative features were developed to clearly identify metastatic breast cancer cells.

4.2. Materials and Methods

4.2.1. Substrate Preparation

Fisher brand microscope slides (12-550D, Fisher Scientific) were cut into 5 mm x 5 mm pieces and used as substrates. Two types of substrates were used. One type was just plane untreated microscope glass slides. The second type consisted of nanotextured slides, produced by reactive ion etching (RIE). Technics Micro-RIE Series 800 Plasma System was used to do RIE. A gas mixture of 10 sccm O_2 and 15 sccm of CF_4 was used in RIE for 25 minutes to create the nanotexture. The RF power was set at 200 W during RIE. Nanotextured substrates were marked to easily separate them from plane ones.

4.2.2. Substrate Topography Examination

Roughness was measured by atomic force microscope (AFM). Non-contact AFM mode was used (Park XE70 AFM) to collect topographical data. Maximum tip diameter was less than 10 nm. Nominal force constant and resonance frequency were 42 N/m and 330 kHz, respectively. Five samples for each type of substrates were scanned and plane levelled. Average, RMS roughness, and maximum peak to valley height were measured.

A Hitachi S-3000N variable pressure scanning electron microscope (SEM) was used to examine the surfaces of nanotextured substrates. The substrates were coated with 5 nm gold film and acceleration voltage of 18 kV was used to capture micrographs.

4.2.3. Surface Elemental Analysis

Elemental analysis of the substrates was done with the energy-dispersive x-ray spectroscopy (EDS) tool of the SEM. It quantified elemental composition of the substrates at low vacuum and 30 kV acceleration voltage.

4.2.4. Contact Angle Measurements

Contact angles of plane and nanotextured substrates were measured with ramé-hart contact angle goniometer (NRL-100; Ramé-hart Instrument Co, NJ, USA). Deionized (DI) water sessile drop was placed on the substrates at room temperature and contact angles were visually observed through microscope at the water-substrate interface. Five measurements were taken for each of total 7 runs.

4.2.5. Substrate Functionalization

Same as described in Chapter 3.

4.2.6. Aptamer Preparation and Substrate Functionalization with Aptamer

Same as described in Chapter 3.

4.2.7. Target Cell Preparation

Same as described in Chapter 3.

4.2.8. Cell Suspension and Image Capture

Around 200,000 cells were present in 1 ml of PBS. A volume of 30 µl of cell solution was loaded on a substrate. Five minute was given for the cells to interact with aptamer modified substrates. The cells were then tracked and imaged with optical microscope for 15 minutes.

4.2.9. Cell Contour Detection

Same as described in Chapter 3.

4.2.10. Distance Matrix Analysis

We compared cell shapes over time and defined distance analysis and shape dissimilarity matrices to objectively detect shape change of cells. Distance matrix analysis is a

standard pattern recognition technique. This technique computes shape change and presents a distance value. Distance value represents shape dissimilarity. Usually the higher the distance value, the more the shape is changing. We converted optical images into binary images having only one of two values: a black pixel or a white one. A black pixel meant presence of cell body at those coordinates and white meant absence. A 2X2 contingency table was generated for each pixel. There were 4 conditions in the table that were derived from the presence of a cell in any two consecutive images. An "*a*" meant presence in both images. The "*b*" depicted presence in first image but absence in next image. The "*c*" was absence in the first image and presence in next image, and absence in both images was recorded was a "*d*". For a particular pixel, only 1 of the 4 conditions had to be true. Using this table, a distance matrix called Jaccard distance was calculated. Jaccard distance is calculated as [109]:

$$Jaccard\ distance = 1 - \frac{a}{a + b + c}$$

Hausdorff and Mahalanobis distance calculation is described in Chapter 3.

4.2.11. Statistical Analysis with Distance Values

Change in distance values were calculated between two following time points for each cell. At the end of 15 min all the changes were summed up to find total distance change for each cell. The average of total distance indicated how the group (metastatic or non-metastatic cells) behaved in terms of morphological change after 15 min. Two tailed *t*-test was used to assess if the averages of any two groups were statistically significant. We calculated *p*-values in each case. We calculated cell shape change ratio using the following formula:

$$Cell\ Shape\ Change\ Ratio_{(Distance,Substrate)} = Distance_{Jaccard\ |\ Hausdorff\ |\ Mahalanobis} of\ Non-Metastatic\ Cells_{Substrate} / Distance_{Jaccard\ |\ Hausdorff\ |\ Mahalanobis} of\ Metastatic\ Cells_{Substrate}$$

where *Distance* was either of the Jaccard distance or Hausdorff distance or Mahalanobis distance, and the *Substrate* was either plane or nanotextured substrate.

4.3. Results and Discussion

4.3.1. Substrate Topography Examination

Roughness values for plane and nanotextured substrates are presented in Table 4-1. AFM micrographs in Fig. 4-1(a-b) show surface features of both types of substrates. On average, nanotexturing increased the RMS roughness from ~6.8 nm (S.D.=3.3 nm) to ~36 nm (S.D.=4.9 nm). Increased roughness directly affected and amplified density of immobilized surface-tethered ssDNA and anti-EGFR aptamer on nanotextured substrates [90]. SEM micrograph of nanotextured substrate is shown in Fig. 4-1(c).

Table 0-1: Substrate Roughness from AFM

Substrate	Average Roughness (nm)±S.D.	RMS Roughness (nm)±S.D.	Maximum Peak to Valley Height (nm)±S.D.
Plane	5.76 ± 4.03	6.87 ± 3.3	28.11 ± 12.2
Nanotextured	29.75 ± 4.57	36 ± 4.9	134.5 ± 13.3

4.3.2. Elemental Analysis of Substrates

Elemental analysis of plane and nanotextured substrates showed that there was no change in the composition of the substrates after RIE (Fig. 4-2). This eliminated any

possible effects on cell behavior due to elemental changes. Trace amounts of C, Al, and K were found on both substrates, which were typical and came from sample handling.

4.3.3. Contact Angle Measurements

Contact angle data shows that the substrates became more hydrophilic after nanotexturing (Table 4-2). Hydrophilic substrates are ideal for biological molecule adhesion [110]. Hydrophobic substrates deter cell attachment while hydrophilic substrates permit and even boost attachment [111-116]. Contact angle values shown in Table 4-2 manifest that nanotexturing increased hydrophilic behavior of the substrates and enhanced interactions between substrates and cells.

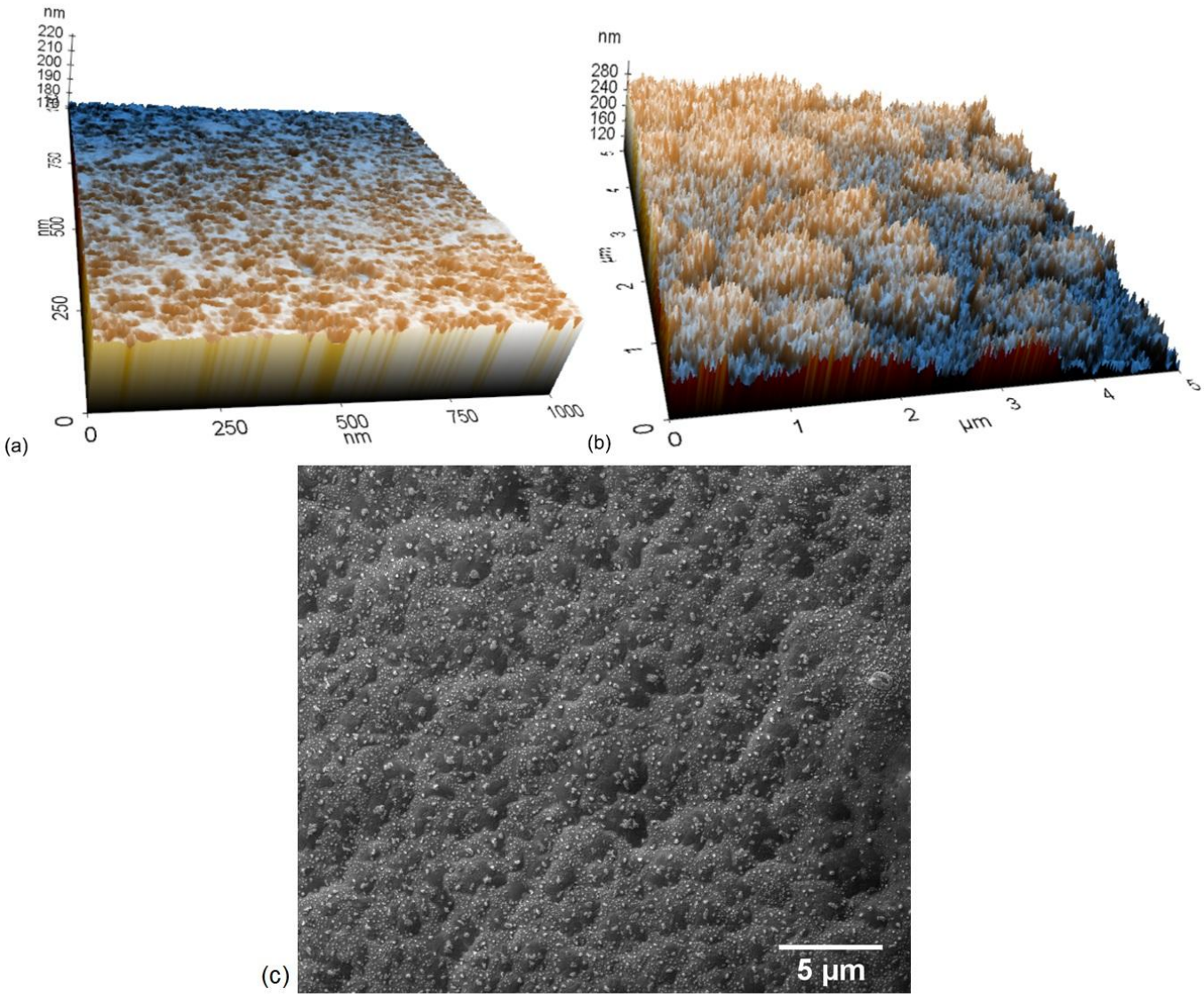

Figure 0-1: AFM micrographs of (a) plane substrate before RIE, (b) nanotextured substrate after RIE. (c) SEM micrograph of the nanotextured substrate.

Table 0-2: Contact Angle Measurements (n=7)

Substrate	Contact Angle ± S.D.
Plane	25° ± 1.5
Nanotextured	12° ± 1

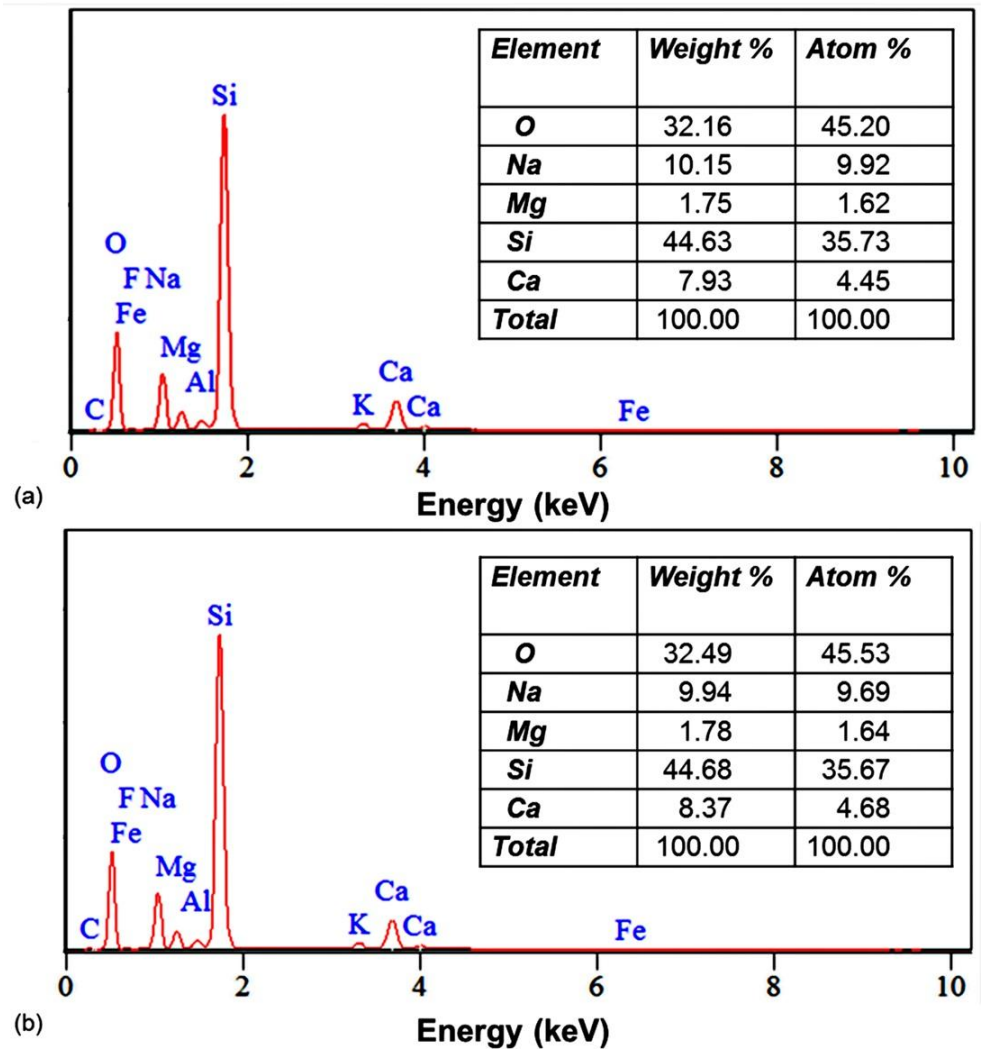

Figure 0-2: EDS analysis of (a) plane and (b) nanotextured glass substrates before chemical and biological modifications.

4.3.4. Cell Morphology Observations

Cells captured on plane and nanotextured substrates were imaged for 15 minutes. Binary images of the cells were extracted from optical images. Fig. 4-3 shows representative cell behaviors observed in the images. Each panel shows one cell at a time, imaged at interval of 3 minutes going from left to right. The data clearly shows that the non-metastatic cells (Fig. 4-3(c-d)) captured on plane and nanotextured substrates did not show significant shape change. Metastatic cells changed their shapes more prominently on nanotextured substrates (Fig. 4-3(a)) than on plane substrates (Fig. 4-3(b)).

Prominent morphological changes of metastatic cells on anti-EGFR aptamer modified nanotextured substrates can be linked with the overexpression of EGFR on cell membrane. EGFRs of cell membrane are activated when captured on nanotextured substrates with anti-EGFR aptamers. Activated EGFR triggers PLC γ, an enzyme dependent intracellular signaling pathway, which influences cell motility [117-119]. Here, we detected shape change of cells from optical images and converted these changes into numeric values to objectively differentiate between metastatic and non-metastatic cells.

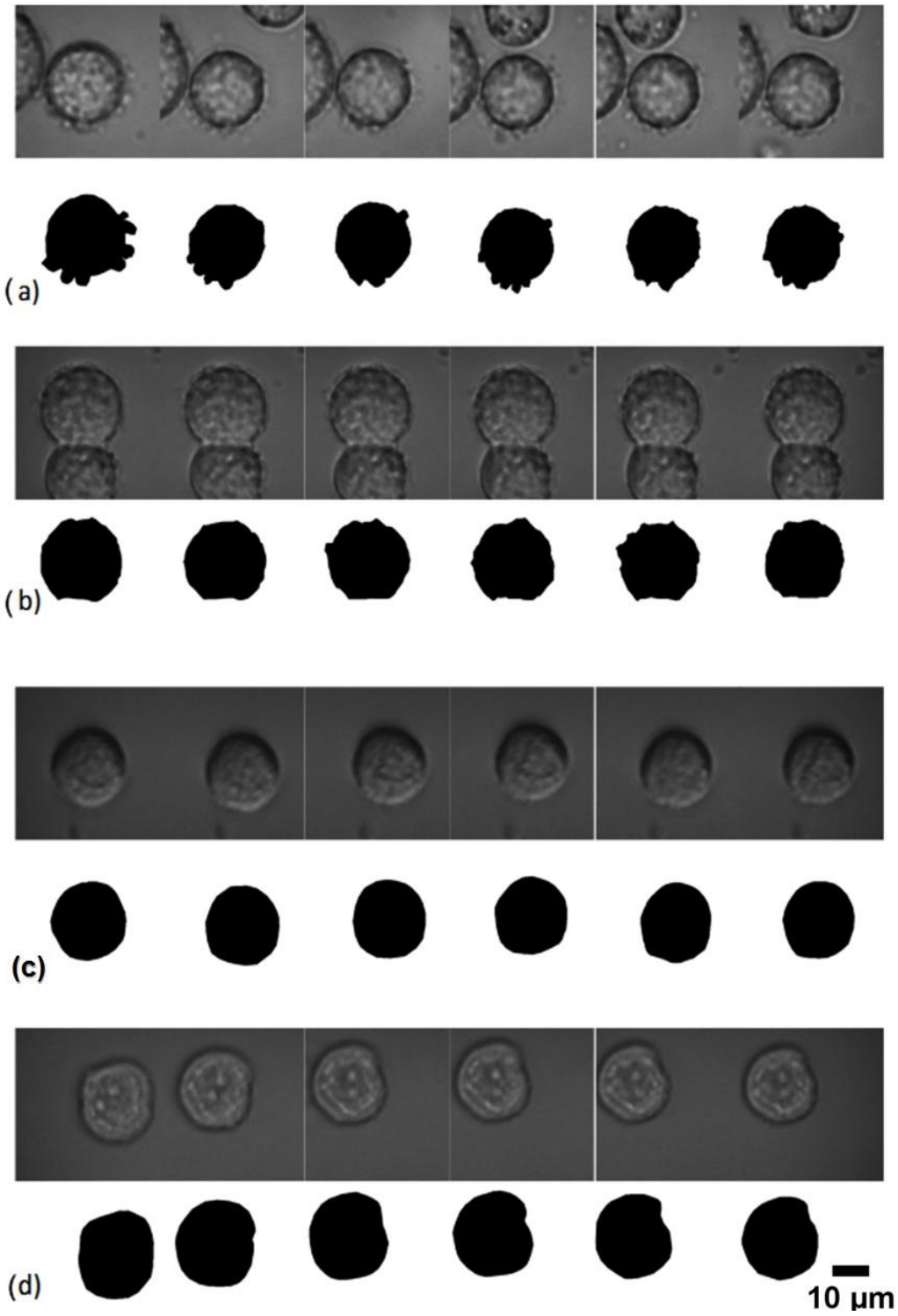

Figure 0-3: Cell behavior over 15 minutes. Going from left to right, each consecutive image is taken at 3 minute mark. The optical and binary images of (a) a metastatic cell captured on nanotextured substrate; (b) a metastatic cell captured on plane substrate; (c) a non-metastatic cell captured on nanotextured substrate; and (d) a non-metastatic cell captured on plane substrate.

4.3.5. Distance Matrix Analysis: Jaccard Distance

For higher dissimilarity in shape, Jaccard distance has higher values. A sensitive detection platform is capable of rendering statistically significant values using simple operations. Jaccard distance value gives a clear measure of the sensitivity of nanotextured functionalized substrates in distinguishing between metastatic and non-metastatic cells. In Fig. 4-4(a), we see that on plane substrates, the Jaccard distance does not show difference between metastatic and non-metastatic cells (both averages ~3.8 a.u.; both S.D.s ~1.2 a.u.). But on nanotextured substrates the disparity is statistically significant and metastatic cells are easily distinguishable (*, p-value < 0.001). Average for metastatic cells is 4.6 a.u. (S.D.=1.2 a.u.) and non-metastatic cells is 2.5 a.u. (S.D.=0.39 a.u.) on nanotextured substrate. Non-metastatic to metastatic cell shape change ratio jumped from 1:1.01 to 1:1.81 for Jaccard distance from plane to nanotextured substrate. Evidently, nanotextured anti-EGFR aptamer modified substrates are remarkably sensitive in detecting metastatic cells from non-metastatic cells than plane functionalized substrates. This shows the compound effect of aptamer interactions and nanotexture.

Overactive extension and retraction of cell membrane for metastatic cells captured on anti-EGFR aptamer modified nanotextured substrates resulted in higher Jaccard distance value than that for non-metastatic cells. Metastatic cells are more flexible than benign cells because of their cytoskeleton structure [120-122]. The agility of actin cytoskeleton structure is thus the vital component in defining vigorous cell membrane extension/retraction of metastatic cells [123, 124].

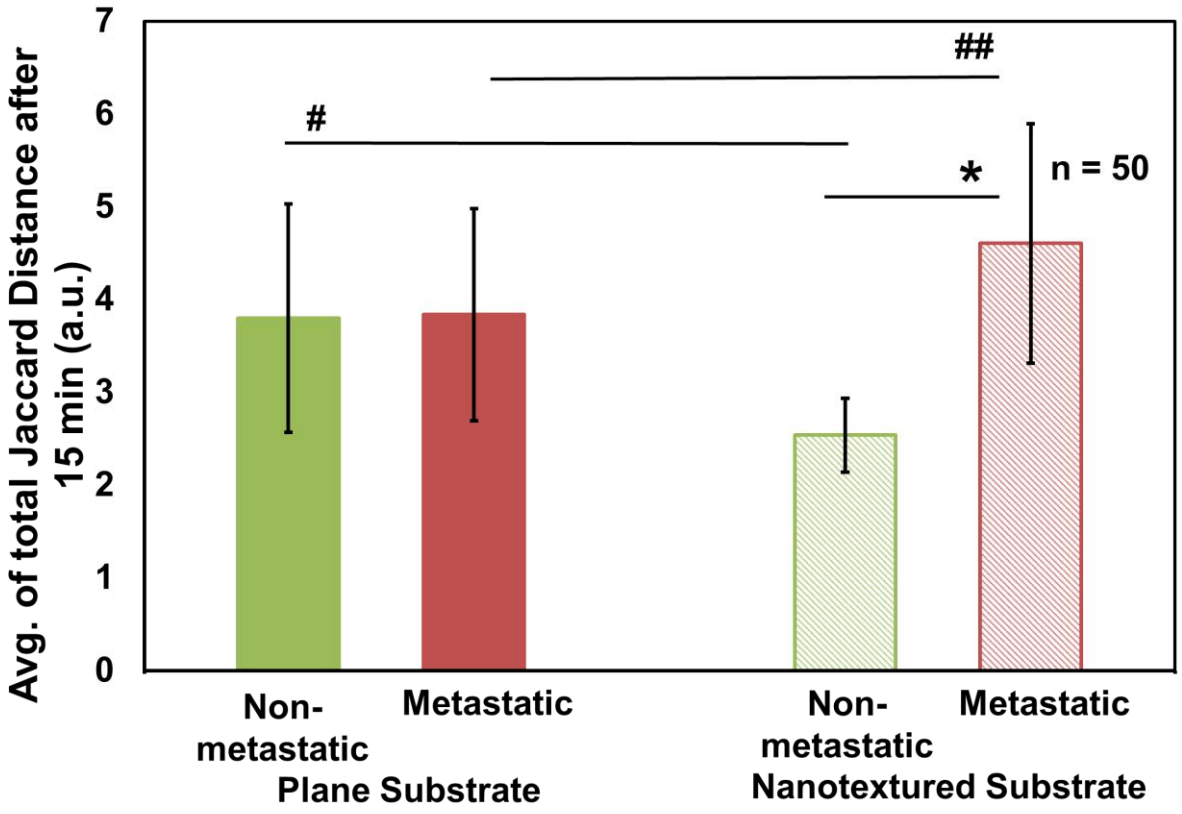

Figure 0-4: Jaccard distance shows dissimilarity from shape change of non-metastatic and metastatic cells on plane and nanotextured substrates (From two-tailed *t*-test; *, *p*-value < 0.0001; #, *p*-value = 0.02; ##, *p*-value = 0.2).

4.3.6. Distance Matrix Analysis: Hausdorff Distance

Hausdorff distance calculation is fast, simple and tolerant of positional errors. This distance value is very rigorous and precise in calculating small positional change. If cells do not change shape, Hausdorff distance value is very low and vice versa. In Fig. 4-5, the averages of total Hausdorff distance changes for cells are plotted. On the plane substrates, metastatic cells showed higher Hausdorff distance; i.e. higher dissimilarity than non-metastatic cells (**, *p*-value < 0.05). The distance value is larger because metastatic cells were rapidly changing shape. On nanotextured substrates, difference

between distance values of metastatic and non-metastatic cells was even higher (*, *p*-value < 0.0001). Average of total distance for non-metastatic cells decreased from 270.4 a.u. (S.D.=118.5 a.u.) to 220.8 a.u. (S.D.=76.25 a.u.) going from plane to nanotextured substrates. Opposite effect was seen on metastatic cells as average of total Hausdorff distance increased from 399.1 a.u. (S.D.=69.3 a.u.) to 484.7 a.u. (S.D.=67.7 a.u.) going from plane to nanotextured substrates. Nanotexture significantly enhanced the activity of metastatic cells while suppressed the activity of non-metastatic cells. As metastatic cells had more EGFR on the cell membranes, they got vigorously active to create more bonds with high density aptamer molecules functionalized on nanotextured substrates. The non-metastatic cells with low density of EGFR on cell membrane got inactive precisely for the same reason. Non-metastatic to metastatic cell shape change ratio improved from 1:1.48 to 1:2.19 for Hausdorff distance analysis going from plane to nanotextured substrate. Undoubtedly, nanotexturing has increased the detection possibility of metastatic breast cancer cells on anti-EGFR aptamer functionalized substrates.

Overactive extension and retraction of cell membrane for metastatic cells captured on anti-EGFR aptamer modified nanotextured substrates resulted in higher distance value than that for non-metastatic cells. Metastatic cells are more flexible than benign cells because of their cytoskeleton structure [120-122]. The agility of actin cytoskeleton structure is thus the vital component in defining vigorous cell membrane extension/retraction of metastatic cells [123, 124].

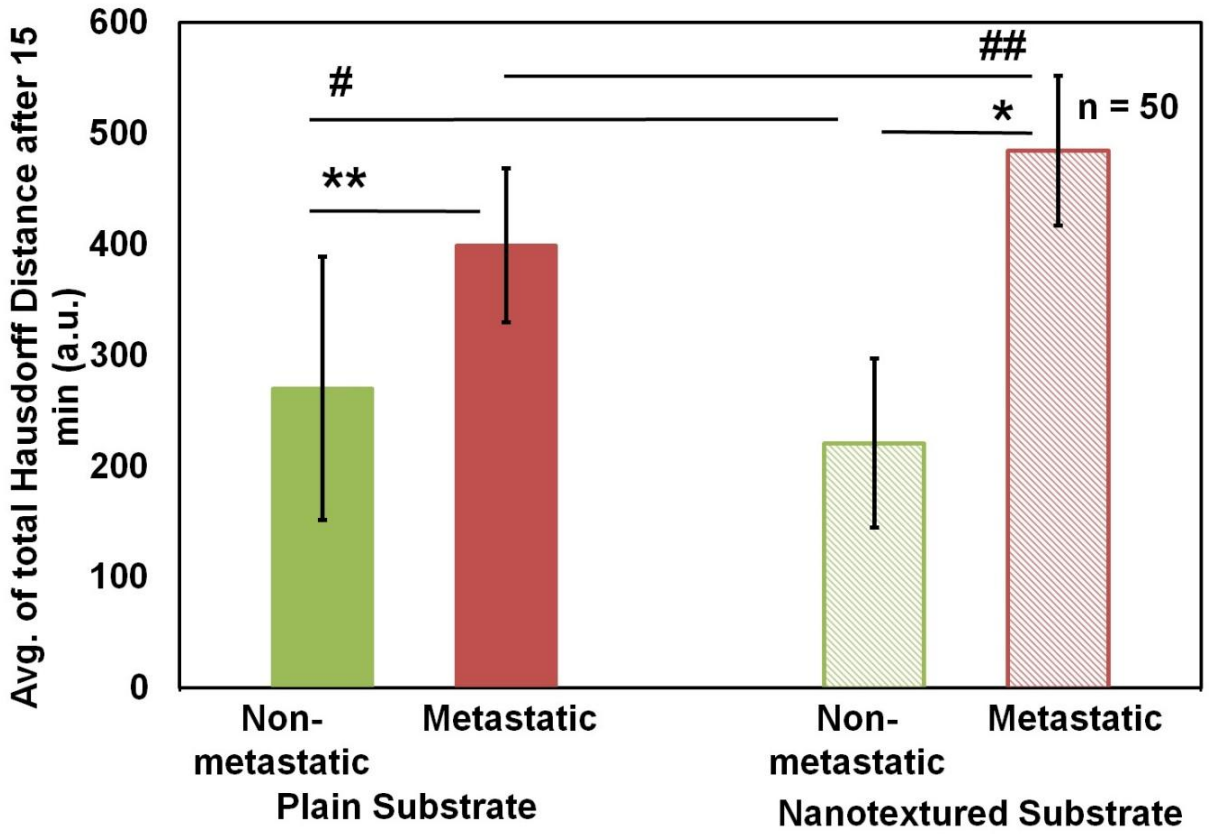

Figure 0-5: Hausdorff distance analysis for shape dissimilarity analysis of the cells (From two-tailed *t*-test; *, *p*-value < 0.0001; **, *p*-value = 0.0007; #, *p*-value = 0.2; ##, *p*-value = 0.006)

4.3.7. Distance Matrix Analysis: Mahalanobis Distance

Mahalanobis distance of a changing cell boundary was calculated. Larger Mahalanobis distance meant larger change in cell boundary. This is evident from Fig. 4-6. The distinguishing factor between metastatic and non-metastatic cells is the difference in their respective average distances. On plane substrates, average distances are 0.49 a.u. (S.D.=0.21 a.u.) and 0.92 a.u. (S.D.=0.2 a.u.) for non-metastatic and metastatic cells, respectively (**, *p*-value < 0.05). On nanotextured substrates, the statistical significance is enhanced, going from 0.32 a.u. (S.D.=0.13 a.u.) to 1.53 a.u. (S.D.=0.34 a.u.) for non-

metastatic to metastatic cells (*, *p*-value < 0.0001). Nanotexture amplified the morphology change of metastatic cells to such extent that Mahalanobis distance analysis clearly differentiated between the behavior of metastatic cells on plane and nanotextured substrates (##, *p*-value = 0.0003). The non-metastatic to metastatic cell shape change ratio improved from 1:1.87 to 1:4.69 for Mahalanobis distance analysis going from plane to nanotextured substrate.

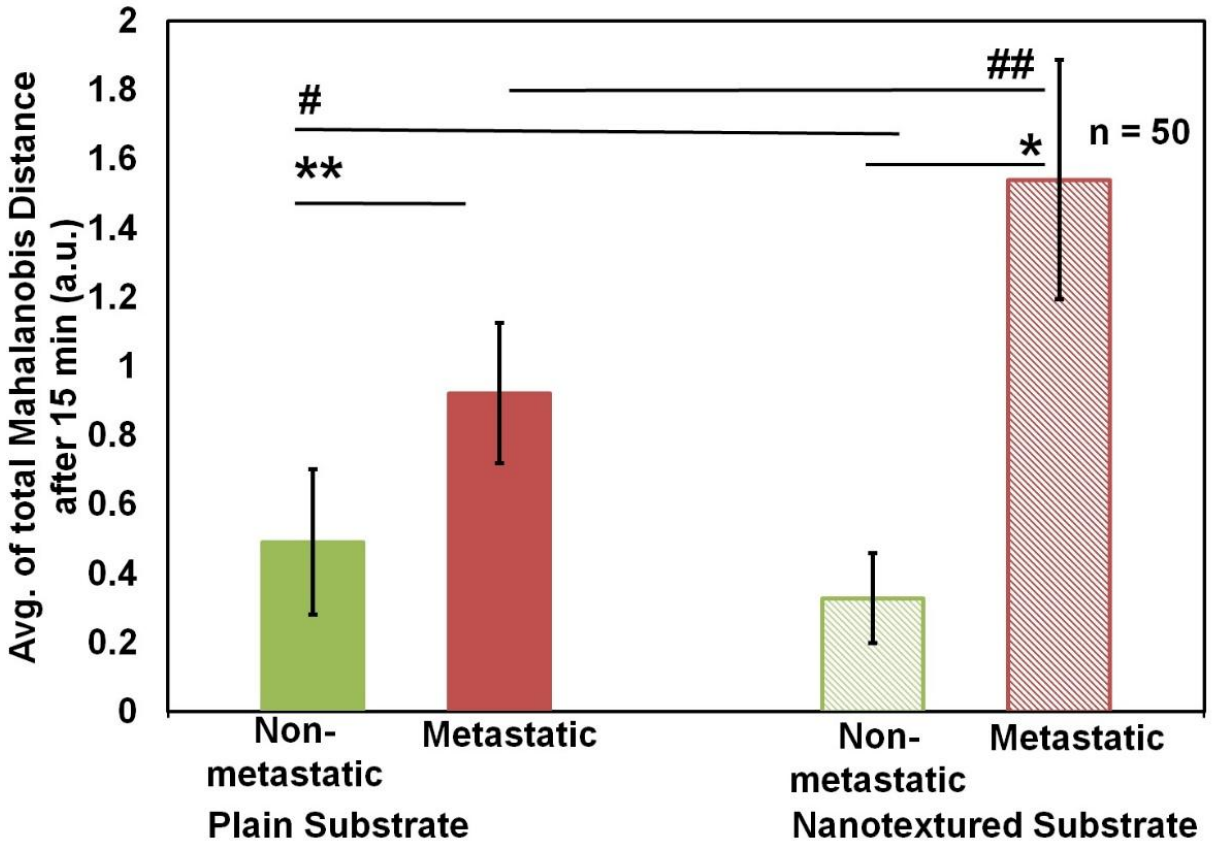

Figure 0-6: Mahalanobis distance analysis showing dissimilarity in the shape of the cells (From two-tailed *t*-test; *, *p*-value < 0.0001; **, *p*-value = 0.001; #, *p*-value = 0.02; ##, *p*-value = 0.0003)

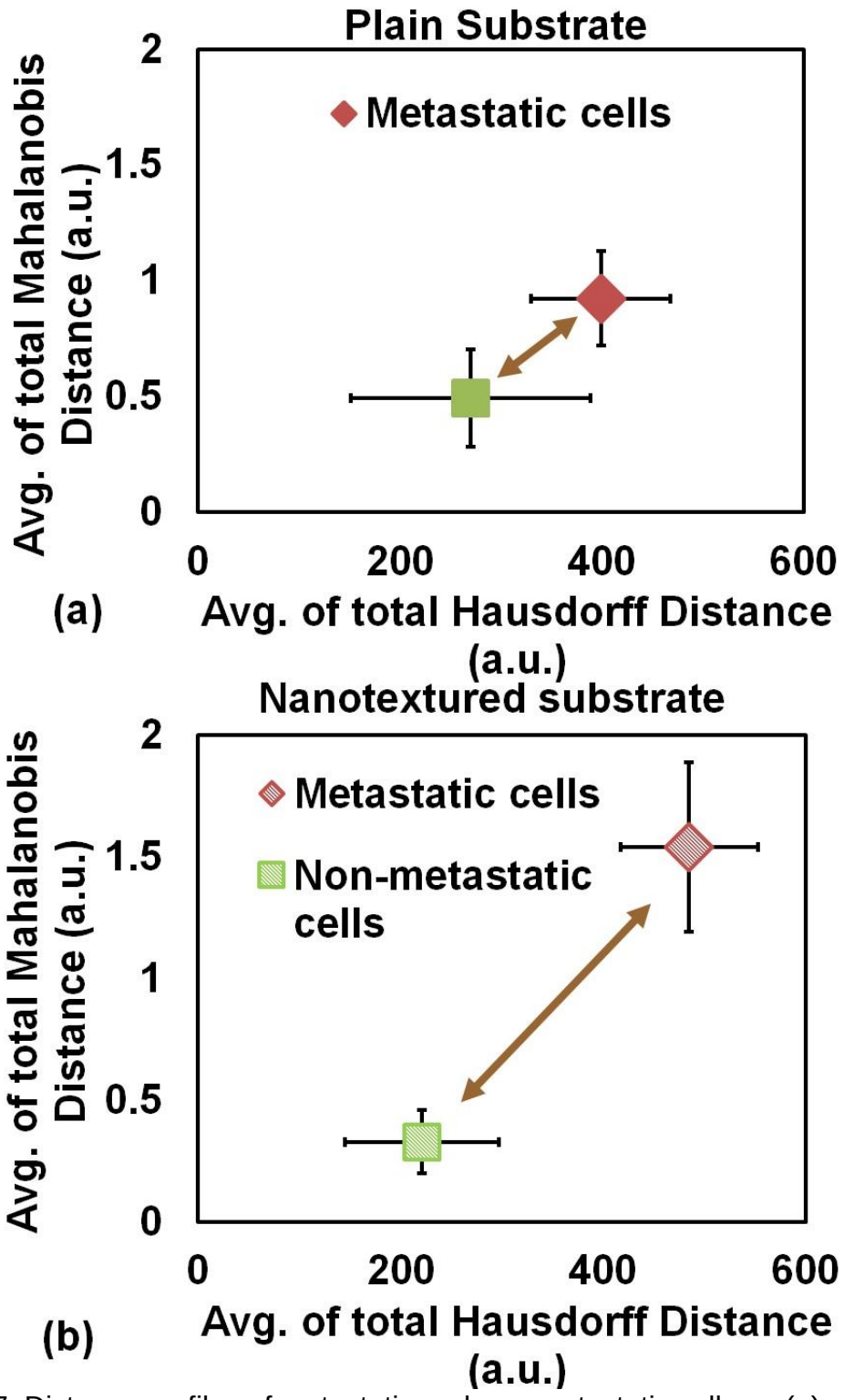

Figure 0-7: Distance profiles of metastatic and non-metastatic cells on (a) plane and (b) nanotextured substrate. Nanotexturing increased the propensity of metastatic cell shape change and induced higher value distance profile. The arrows show contrast between metastatic and non-metastatic cells. Detection efficiency is increased for metastatic cells on anti-EGFR aptamer modified nanotextured substrates.

In Fig. 4-7, the distance profiles for metastatic and non-metastatic cells are summarized to show the enhancement in contrast. It is evident that the differentiation between metastatic and non-metastatic cells is amplified on nanotextured anti-EGFR aptamer modified substrate.

Another advantage of nanotextured substrate over plane substrate is that it has effectively more surface area [107]. Hence, more number of linker ssDNA and thus RNA aptamer molecules are tethered on nanotextured substrates. Capture efficiency has already been reported to go up for cancer cells on nanotextured substrates [107]. There is thus more to nanotexture than just surface area. In this work, the shape change phenomena of cancer cells on aptamer modified nanotextured substrates has been investigated and quantifiable differentiation metrics have been defined to categorize metastatic cells from non-metastatic ones.

Differentiating metastatic cell from non-metastatic ones is critical for cancer staging to define appropriate treatment regime. The fabrication process for the glass substrate is easy, economic and scalable. The capture process is selective, efficient and label-free [94]. The aptamer modified nanotextured platform enhance cell motility which is a novel and easy physical biomarker for early detection. Established distance profiles for metastatic and non-metastatic cells provide simple metrics for objective and error-free differentiation. Overall, the implementation of nanotextured functionalized platform with optical image analysis yielded an innovative strategy for sensing metastatic breast cancer cells in a simple and economic setting.

4.4. Conclusions

Early detection of metastatic breast cancer is important for effective therapy and reduced mortality rates. The main challenge is to distinguish metastatic cells from non-metastatic ones. This work presents a nanotextured platform and analysis approaches for rapid, robust and objective detection of metastatic cells from non-metastatic ones. Results demonstrated that aptamer modified nanotextured substrates substantially enhanced the morphological changes of captured metastatic cells. This physical attribute can be used as cellular biomarker for metastatic cancer cell detection. The quantification produced statistically significant difference between metastatic and non-metastatic cell features. Functionalized nanotextured substrates integrated with the image processing and analysis methods can be thus incorporated in effective point of care devices for affordable and quick detection of metastatic breast cancer.

Chapter 5

DETECTION OF CANCER METASTASIS BY DISTANCE MATRIX ANALYSIS FROM SURFACE IMMOBILIZED TUMOR CELLS IN BLOOD

5.1. Introduction

Recently we have demonstrated increased cell capture efficiency with nanotextured substrates [56, 57, 108]. Nanotexturing offers increased surface area for binding to a high quantity of proteins or nucleic acids. Several studies already demonstrated that cell capture, cell growth, adhesion and orientation are influenced by nanoscale topography of surfaces [91]. We have also observed previously that glioblastoma cells show distinctive morphological change with time on aptamer grafted substrates [94, 95]. We report quantitative analysis of the shape change of tumor cells with respect to normal blood cells. We calculated distance matrices to evaluate the shape change feature and compare tumor cells with blood cells. Tumor cells exhibited higher shape change and presented a distinguishable profile from blood cells. We used this distance profiles to detect tumor cells from blood. This approach can be a prospective platform towards functional and accurate point of care devices for label free CTC detection in breast cancer patients.

5.2. Materials and Methods

5.2.1. Substrate Preparation

Same as described in Chapter 4.

5.2.2. Substrate Topography Characterization

Same as described in Chapter 4.

5.2.3. Substrate Composition and Contact Angle Analysis

Same as described in Chapter 4.

5.2.4. Aptamer Preparation and Surface Functionalization

Same as described in Chapter 4.

5.2.5. Target Cell Preparation and Blood Collection

Metastatic breast cancer cell line MDA-MDB-231 was used as a model for cancer cells. These cells have overexpression of EGFR and the tyrosine kinase receptors on the membrane were targeted to capture the cells with anti-EGFR functionalized nanotextured substrates. The cells were obtained from the University of Texas Southwestern Medical Center at Dallas, Texas. Cells were cultured in Dulbecco's modified Eagle's medium (DMEM/F-12, Cellgro, Corning) with 10% heat inactivated fetal bovine serum. L-glutamine and Gentamycin were added to the medium in a sterile humidified environment (95% air, 5% CO_2 at 37 °C). Cultured cells were centrifuged and diluted with sterilized warm 1× PBS. The prepared cells were immediately used.

The blood samples were collected from the tail of a rat after restraining it. K2-EDTA was used as anti-coagulant.

5.2.6. Dynamic Tracking of Metastatic Cancer and Blood Cells

The metastatic breast cancer cells were suspended in 30 µl PBS solution and placed on functionalized nanotextured substrates. There were ~200,000 cells in 1 ml of PBS. The cells were captured on the functionalized substrates. After the cells settled down, optical images were taken for 15 minutes at 30 seconds interval.

Blood sample taken from rat tail was used to extract white blood cells (WBC). Red blood cell (RBC) lysis buffer was used to lyse RBCs. Ten ml of 1x RBC lysis buffer was added to each ml of blood. The solution was then incubated at room temperature for 10 minutes with occasional shaking. Chemical reaction was stopped by adding 10 ml of 1x PBS to the solution. The solution was then centrifuged at 300g for 5 minutes and the pellet was resuspended in 1x PBS. RBCs of blood were lysed by then and only WBCs were left. The intact WBCs could be seen along with debris of RBCs through the microscope. Cell suspension of WBCs was loaded on the nanotextured functionalized substrates and cells were again tracked for 15 minutes and images were taken after every 30 seconds.

5.2.7. Tumor Cell Detection from Blood

The rat blood was spiked with metastatic breast cancer cells. One hundred µl of rat blood was mixed in 15 ml of 1x PBS. From diluted blood, 500 µl was taken and set aside. It is reported that, the concentration of WBC is 6000 cells in 1 µl of rat blood [125]. In the set aside volume, around 20,000 WBCs were present. Metastatic breast cancer cells (MDA-MDB-231) were suspended in 100 µl of 1x PBS. The cell concentration was 20,000 cells per 100 µl. The diluted blood and metastatic cell suspension were mixed together. This suspension had 20,000 cancer cells and 20,000 WBCs; a ratio of 1:1. A 50 µl aliquot of this mixture was suspended on nanotextured functionalized substrate. The substrates were images for 15 minutes at 30 seconds interval. The experiments were repeated six times.

5.2.8. Image Analysis

Same as described in Chapter 4.

5.3. Results and Discussion

5.3.1. Substrate Topography Evaluation

Same as described in Chapter 4.

5.3.2. Size Comparison between Blood Cells and Metastatic Cancer Cells

We compared size of blood cells and metastatic breast cancer cells. In Fig. 5-1(a) blood spiked with tumor cells is shown. Diameters for RBCs, WBCs and tumor cells are shown in Fig. 5-1(b). Average diameter of RBCs, WBCs and tumor cells were 4.9 µm (S.D.=0.6 µm), 7.8 µm (S.D.=1.8 µm), and 13.5 µm (S.D.=1.8 µm) respectively. Among the cells RBCs are too small enough to be visually detected. Moreover, they are concave or disk shaped [125]. Lymphocytes make 86% of all WBCs and have diameters between 6 to 15 µm [125]. Tumor cells and WBCs have the same diameter range depending on cell maturity. For easy interpretation of results, we eliminated RBCs because of their easy detection due to smaller diameter and visible disk shape. We compared WBCs with tumor cells based on their shape changes on nanotextured aptamer modified substrates.

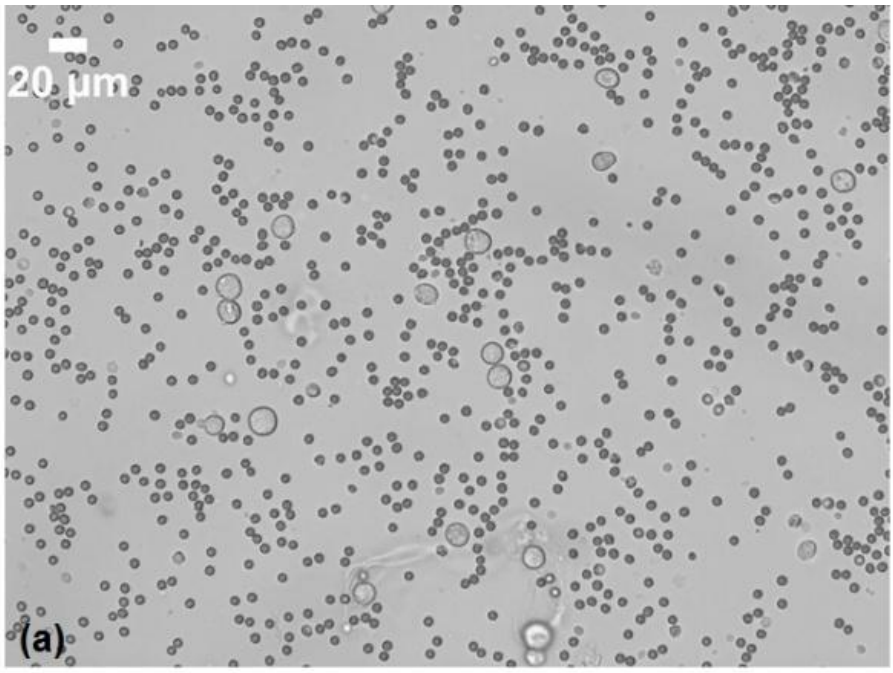

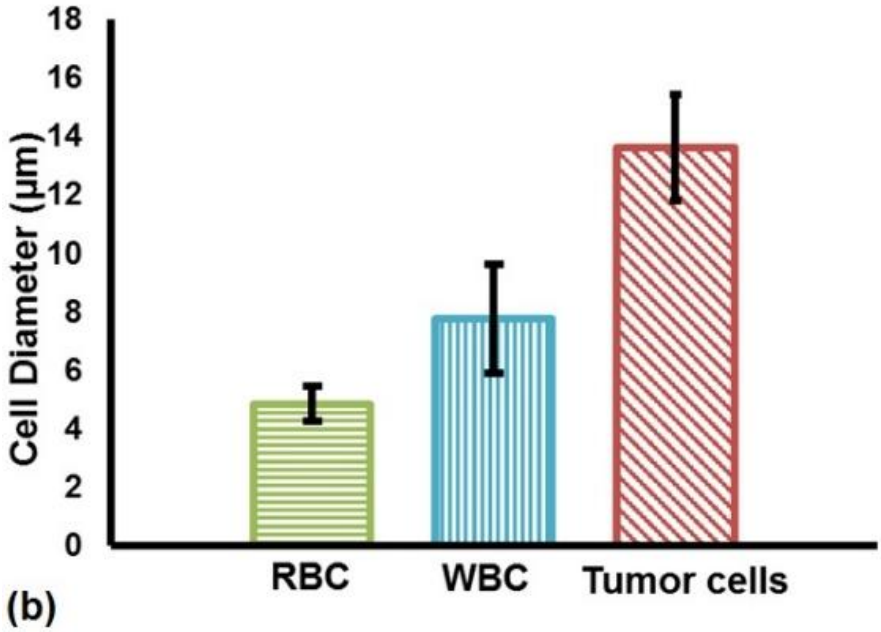

Figure 0-1: Size comparison between tumor cells and blood cells. (a) Blood spiked with tumor cells on aptamer modified nanotextured substrate. (b) Cell diameter of rat RBCs, WBCs and tumor cells. WBCs and tumor cells are almost the same size. (n=30 for each type of cell)

5.3.3. Dynamic Tracking of Captured Cells on Functionalized Substrates

The tumor cells suspended in 1x PBS solution were captured on nanotextured aptamer grafted substrates and imaged for 15 minutes. Same steps were followed for WBCs extracted from blood through lysis. From the images of tumor cells and WBCs, it was observed that only tumor cells changed cell shape with time. Cell membrane on tumor cells created tiny processes like filopodia and lamellipodia. These projections were not static rather they changed position and size with time. The WBCs were inactive from this perspective. Representative cell shape changes are shown in Fig. 5-2. Fig. 5-2(a) shows filopodia/lamellipodia extensions and retractions of tumor cells over time. Fig. 5-2(b) shows comparatively static and inactive WBCs.

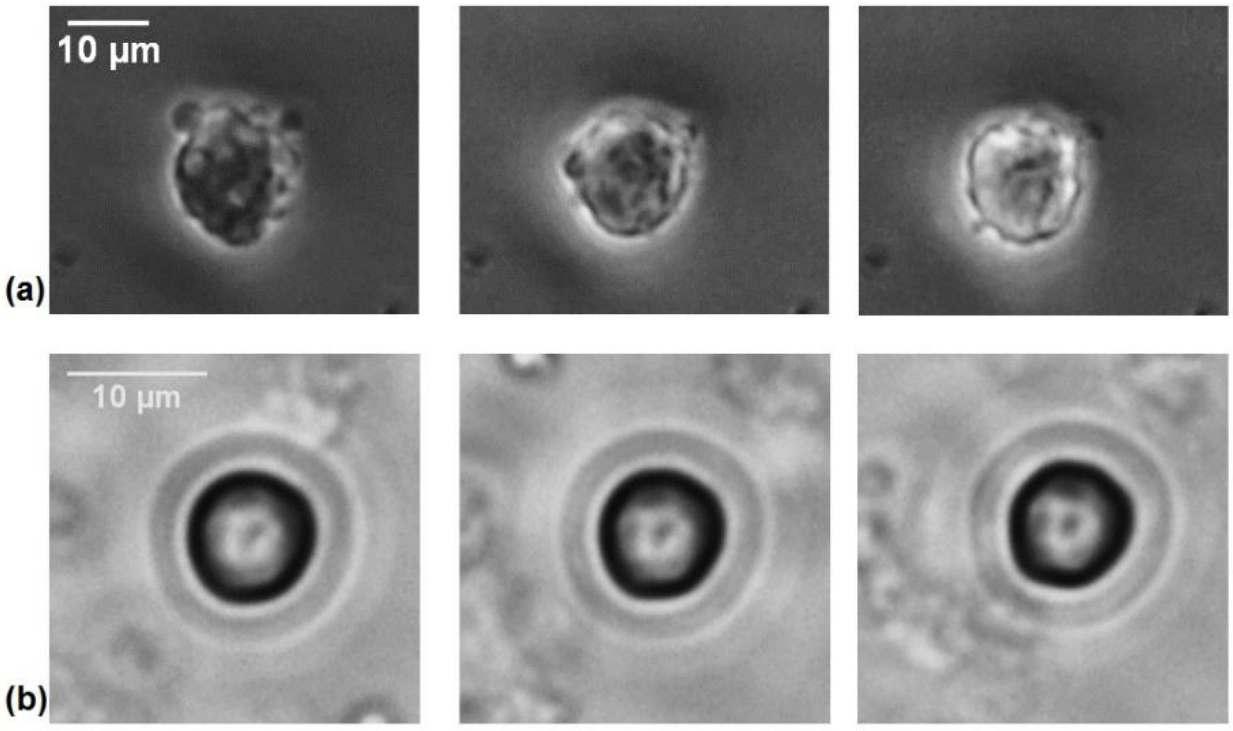

Figure 0-2: Dynamic cell tracking of tumor cell and WBC with respect to time. From left to right each image is taken at 4 minutes interval. (a) Tumor cell changed shape by creating processes. (b) WBC did not show any cell membrane protrusion with time.

5.3.4. Distance Matrix Analysis for Cell Shape Change

We calculated two distance matrices. Distance matrix calculation is standard for comparing shapes of biological objects [126]. The first matrix was the Hausdorff distance [97]. In Fig. 5-3(a), Hausdorff distance changes for tumor cells and WBCs are plotted with respect to time. Tumor cells captured on aptamer grafted nanotextured substrates are uniformly showing higher Hausdorff distance than WBCs.

The second distance matrix was Mahalanobis distance. Larger Mahalanobis distance meant larger change in cell boundary or cell shape. From Fig. 5-3(b) it is evident that tumor cells again are continuously changing cell shape compared to indolent WBCs.

Nanotopography have been known to influence the organization of focal adhesions, the sites of transmembrane integrin clustering, by prompting specific integrin recruitment [127]. Nanotexture induces orientation of actin filaments, microtubules or localization of focal adhesion proteins and hence controls cell motility, alignment, and attachment [128-135]. On the other hand, altered cellular motility instigated by genetic mutation and abnormal expression of cytoskeletal proteins is a hallmark feature of metastatic cancer [136, 137]. In numerous invasive cancer types, Rho GTPase genes are upregulated, These genes control Rho GTPase signaling pathway which regulates the cytoskeleton [138]. Rho GTPases are a family of 20 small G proteins. In gastric adenocarcinoma cells, increased activity of a Rho protein results alterations to cytoskeletal organization stimulating amoeboid-like cell motility [139]. Nestin, an intermediate filaments protein, is overexpressed in metastatic pancreatic and prostate cancer, melanoma and glioblastoma [140]. Overexpression of Vimentin, another intermediate filaments protein, can be correlated with several invasive cancer [141]. Perturbed expression of focal adhesion

kinase, a focal adhesion regulatory protein, is found to be associated with increased progression to highly malignant pathology [142]. It is evident that cancer cells can reorganize cytoskeleton dynamically [143]. Dynamic cell shape change in captured tumor cells was thus amplified by nanotextures on the substrates.

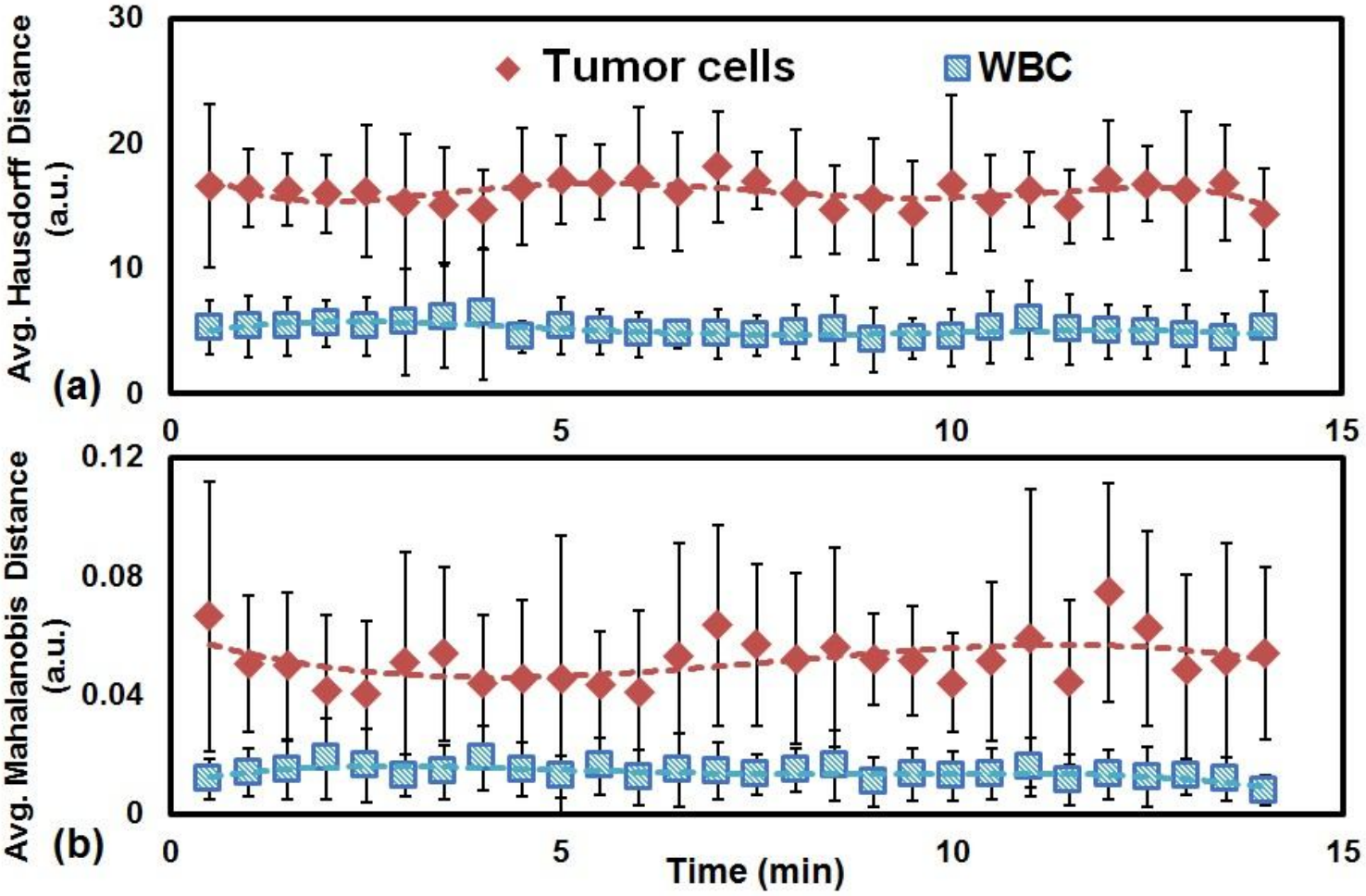

Figure 0-3: Calculated distance matrix of cell shape changes for tumor cells and WBCs. (a) Average Hausdorff distance (b) Average Mahalanobis distance of cells with time. The red markers and fitted curves are for metastatic breast cancer cells, blue markers and blue fitted lines are for WBCs. Metastatic cells show higher distance values meaning higher cell shape changes compared to WBCs (n=32).

5.3.5. Discrimination of Metastatic Cancer and Blood Cells

Distance matrix analysis established that metastatic breast cancer cells were constantly changing shape and showing high distance values with time. After 15 minutes of observation, the total distance values were averaged out for Hausdorff and Mahalanobis distance, respectively (Figs. 5-4 (a-b)). In Fig. 5-4(a) average Hausdorff distance for tumor cell is 451.3 a.u. (S.D.=60.9 a.u.) and WBC is 143.3 a.u. (S.D.=43.6 a.u.). In Fig 5-4(b) average Mahalanobis distance for tumor cell is 1.45 a.u. (S.D.=0.32 a.u.) and WBC is 0.36 a.u. (S.D.=0.113 a.u.). Tumor cells have 214.9% higher Hausdorff distance and 274.7% higher Mahalanobis distance than WBCs. Statistical difference of Hausdorff and Mahalanobis distance between WBCs and tumor cells are significant (p-value < 0.01). The two distances for both tumor cells and WBCs are shown together in Fig. 5-4(c). Tumor cells and WBCs occupy distinguishably separate areas in the plot. The WBCs occupy an area with low distance values and the tumor cells with high distance values. Tumor cells in peripheral blood highly vary in maturity and certainly not all cells would show high distance values practically. In clinical samples we would expect the area occupied by tumor cells in Fig. 5-4(c) to be broader and overlapping with some area of WBCs. But we can expect a high volume of tumor cells to show high distance values and hence easily detectable from their distinguishing distance profile.

5.3.6. Detection of Tumor Cells from Blood

The rat blood was spiked with metastatic breast cancer cells to model tumor cells in peripheral blood. Blood was diluted with 1x PBS and the ratio between tumor cells and WBCs was 1:1. After introduction of cell suspension on EGFR-functionalized

nanotextured substrates and imaging, the distance values for the cells were extracted from binary images, as plotted together in Fig 5-5.

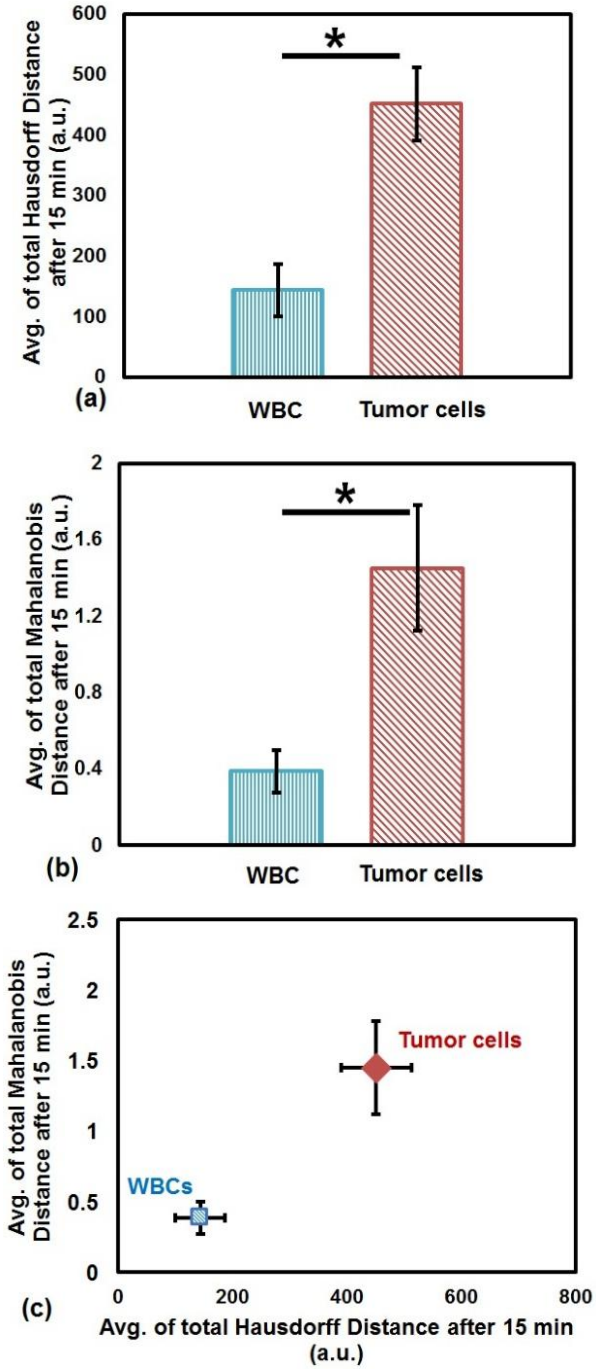

Figure 0-4: Average distance values for WBCs and tumor cells after 15 minutes. (a) Average Hausdorff distance (*, *p*-value < 0.01) and (b) average Mahalanobis distance (*, *p*-value < 0.01). (c) Both types of cells plotted with respect to their distance profiles. WBCs are observed to occupy low distance values and tumor cells to populate high distance values (n=32).

From Fig. 5-1, it could be inferred that the cells with diameter smaller than 6 µm and with disk shapes were indeed RBCs. These cells were eliminated from the results to keep the detection simple. Only WBCs and tumor cells were taken into account. Rat WBCs were slightly smaller in diameter compared to tumor cells (refer to Fig. 5-1).

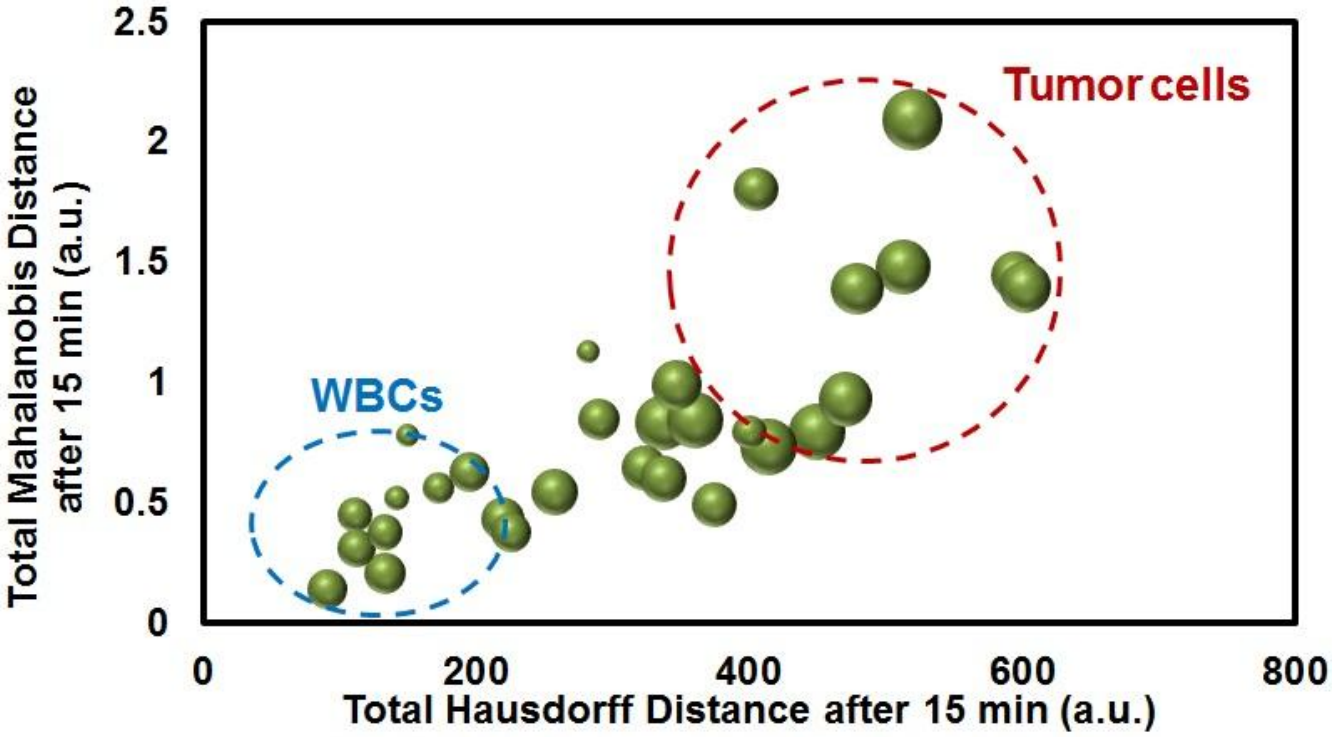

Figure 0-5: Tumor cell detection from blood based on distance profiles. Red dotted line (on the right top) encloses the area occupied by cancer cells based on previous calculations. The blue dotted line encompasses WBC population (lower left area). The sizes of the markers suggest the sizes of respective cells. All larger cells are inside tumor region and smaller cells are inside WBC region. From previous measurements of cell diameters, it is evident that tumor cells are larger than WBCs and are indeed residing in the tumor region.

In Fig. 5-5, the Hausdorff and Mahalanobis distance of the cells captured on 0.5 mm x 0.5 mm substrate are plotted. The red dotted line encloses the already established area for tumor cells from Fig. 5-4(c). The cells in this area make 75% of the tumor cells expected to be captured. The bubble plot represents the distance profiles of the cells and

the the cell diameters. It is noticeable that the cells with high distance profiles also have larger diameter indicating them to be tumor cells. In a similar fashion, cells with low distance profiles (shown inside dotted blue line on lower left corner) have smaller diameters suggesting to be WBCs. There is an overlap region between these two populations. Outside the overlap region 60% cells could be identified as either tumor cells or WBCs, and 75% of tumor cells could be discriminated from blood cells based on their distance profile. Tumor cells are inherently more flexible than healthy cells due to their cytoskeleton structure [120, 121]. The agility of cytoskeleton structure is the vital component in defining vigorous morphology change of these cells.

Detecting tumor cells from peripheral blood is critical for early detection of metastasis. Cell motility on aptamer functionalized nanotextured substrates can be an easy and unique physical biomarker for tumor cell detection. We have previously showed that specific fluid flow rates can dislodge captured cancer cells for collection and further processing [144]. We can incorporate that technique here with our tumor cell detection platform to collect tumor cells after successful detection. Our results showed that combined implementation of functionalized nanotextured platform with distance analysis algorithms yielded an innovative strategy for sensing tumor cells from blood in a simple and economic setting.

5.4. Conclusions

A simple and unique platform is presented here to detect tumor cells from peripheral blood based on their distinguishing distance profiles on anti-EGFR aptamer modified nanotextured substrates. To target EGFR that is overexpressed on tumor cell membrane, anti-EGFR aptamer was grafted on nanotextured substrates. Anti-EGFR aptamer

provided selectivity between blood cells and tumor cells as well as cell cytoskeleton flexibility in tumor cells. We detected >75% of the tumor cells. Given the scarce number of tumor cells present in blood, the whole clinical sample can be suspended on a bigger substrate and a stepper microscope can be used to record images in all locations on the substrate. This technique can be economical as there is no need to use expensive sensing transducers or tedious fabrication methods. Fabrication of nanotextured substrate is simple and yields uniform nanoscale roughness. The functionalization process is widely accepted and standardized with high capture efficiency. The system can be used for any kind of metastatic cancer overexpressing EGFR. Our capture procedure and distance calculation method can be developed in to a cost effective and efficient point of care device to detect metastasis at early stages.

Chapter 6

DEVELOPMENT OF A NON-INVASIVE TEST FOR BLADDER CANCER DETECTION BASED ON CELLULAR TRACKING AND DISTANCE MATRIX ANALYSIS

6.1. Introduction

We have developed a very simple non-invasive technique based on distance matrix analysis on cellular images to detect bladder cancer cells. We captured advanced stage bladder cancer cells on anti-EGFR aptamer coated nanotextured glass substrates. Cancer cells show distinctive morphological behavior on aptamer modified substrates and on aptamer modified nanotextured substrates this behavior is enhanced [145]. We captured urothelial cells and bladder cancer cells on anti-EGFR aptamer modified nanotextured substrates and observed them under an optical microscope for 15 minutes. The healthy urothelial cells did not show any morphological change. But the bladder cancer cells showed characteristic morphological change with time. We could differentiate between healthy and cancerous cells from distance matrix analysis. We employed the representative distance profiles of bladder cancer and urothelial cells among captured cells from bladder cancer patient urine samples on aptamer functionalized nanotextured substrates and detected cancer cells successfully. This technique is very selective, simple, and economic. As the captured cancer cells are label-free, their cellular characteristics are uncompromised and can be detached from the substrate for subsequent analysis. The technique is non-invasive and can be further developed as a platform towards a point of care device for bladder cancer detection from urine.

6.2. Materials and Methods

6.2.1. Substrate Preparation

Same as described in Chapter 5.

6.2.2. Surface Characterization

Same as described in Chapter 5.

6.2.3. Substrate Functionalization

Same as described in Chapter 5.

6.2.4. Human Urothelial Cell Preparation

Human uroepitheliam derived immortalized cell line SV-HUC was used as model for healthy urothelial cell. The cells were cultured with T-medium (Invitrogen) supplemented with 5% fetal bovine serum. Cultured cells appeared as an epithelioid cell monolayer and were enzymatically dissociated with trypsin (0.25%)–EDTA (0.03%) solution. Cultured cells were centrifuged and diluted with sterilized warm 1× PBS and immediately used in the experiments. Cell concentration was 200k in 1 ml PBS.

6.2.5. Human Bladder Cancer Cell Preparation

Human bladder cancer cells (T24) were purchased from American Type Culture Collection (Rockville, MD). Cells were cultured with T-medium supplemented with 5% fetal bovine serum. Trypsin (0.25%)–EDTA (0.03%) solution was used to dissociate the cells enzymatically when the cells were confluent. Trypan blue assay was used to assess the viability of the cultured cells after trypsinization and >94% cells were healthy. These cells have overexpression of EGFR and the tyrosine kinase receptors on the membrane were targeted to capture the cells with anti-EGFR functionalized nanotextured substrates.

Cultured cells were centrifuged and diluted with sterilized warm 1× PBS. The prepared cells were immediately used. The concentration of the cells in suspension was 200k cells per ml.

6.2.6. Patient Urine Sample Preparation

Two urine samples from patients known to have bladder cancer were procured from University of Texas Southwestern Medical Center at Dallas, Dallas, Texas. The two samples were tagged as “sample no. 1” and “sample no. 2”. Sample volume was 50 ml each. The samples were stored inside icebox to carry from collection site to laboratory. Two centrifuge tubes were sterilized for holding the samples. Polypropylene cell strainer (BD Falcon) with a nylon mesh of 100 µm size was used to remove any chunks or cell clumps. Two strainers were pre wet with imaging medium PBS and placed on the mouth of the centrifuge tubes. The samples in carrier containers were gently shaked and the contents were poured through the strainers into the centrifuge tubes. Both filtered samples were centrifuged at 3000 rpm for 5 minutes. Supernatant was removed and 1X PBS was added to make the volume of each tube 200 µl.

6.2.7. Dynamic Tracking of Cells

The urothelial and bladder cancer cells were suspended in 30 µl PBS solution and placed on anti-EGFR aptamer functionalized nanotextured substrates. There were ~200,000 cells in 1 ml of PBS for both types of cells. The cells were captured on the functionalized substrates. After the cells settled down, optical images were taken for 15 minutes at 30 seconds interval.

Cell pellets prepared from patient urine samples were tagged according to sample number. The pellets was suspended on previously prepared anti-EGFR aptamer functionalized nanotextured substrates. After the cells settled down they were observed through the optical microscope and images were taken for 15 minutes at every 30 seconds.

6.2.8. Image Analysis and Data Interpretation

Same as described in Chapter 5.

6.2.9. Hamming Distance Calculation

Morphological changes were measured from segmented binary images. Distance matrices were calculated for cell shape similarity check. Higher distance value meant higher shape change. The values for the distance matrices showed statistically significant differences between healthy urothelial and bladder cancer cells captured on nanotextured aptamer functionalized substrates.

Hamming distance is a metric based on binary segmentation. The cell images were converted to binary for each and every pixel. Hamming distance measured the number of pixels that were different in two consecutive images. It's an exclusive-or (XOR) operation between two cell images followed by a count operation to sum up the number of ones in the XOR result. Table 6-1 shows the XOR operation between images. Hamming distance calculated from XOR operation is:

$$Hamming\ Distance = \sum_{i} x_i \oplus y_i$$

Table 0-1: XOR operation on image. 1 means pixel is present inside/on cell boundary; 0 means pixel is absent inside/on cell boundary.

Pixel value in image (x_i)	Pixel value in consecutive image (y_i)	XOR ($x_i \oplus y_i$)
0	0	0
0	1	1
1	0	1
1	1	0

Hamming distance is widely used to differentiate between cell types based on genetic expression [146-149].

6.2.10. Hausdorff Distance Calculation

Same as described in Chapter 5.

6.2.11. Mahalanobis Distance Calculation

Same as described in Chapter 5.

6.2.12. Statistical Analysis with Distance Values

Same as described in Chapter 5.

6.3. Results and Discussion

6.3.1. Substrate Topography Assessment

Same as described in Chapter 5.

6.3.2. Dynamic Tracking of Urothelial and Bladder Cancer Cells on Functionalized Substrates

In Fig. 6-1, both urothelial and bladder cancer cells are shown after they were captured on anti-EGFR aptamer functionalized nanotextured substrate. Fig. 6-1(a)(I) shows urothelial cells and Fig. 6-1(b)(I) shows bladder cancer cells. From visual observation we saw that urothelial cells were showing uniform cell membrane while bladder cancer cells showed rough membranes. Images were taken over 15 minutes to track cell shape change due to membrane roughness. With time, filopodia/lamellipodia like fine

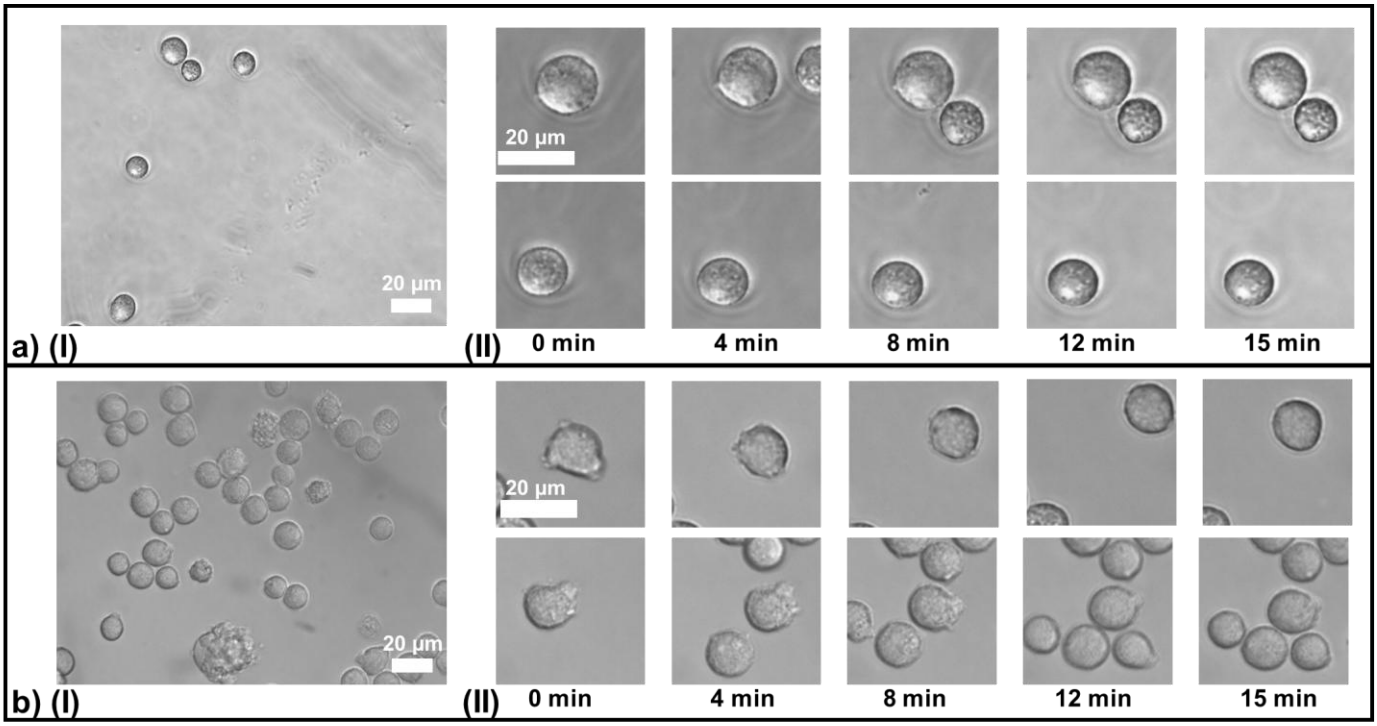

Figure 0-1: (a) Urothelial cells captured on anti-EGFR aptamer coated nanotextured substrate: (I) Urothelial cells showed smooth membrane (II)Time series image of urothelial cells showed, with time the cells maintained their smooth membrane and did not show any morphological change. (b) Bladder cancer cells captured on anti-EGFR aptamer modified nanotextured substrate: (I) Bladder cancer cells showed rough cell membrane (II) With time filopodia/lamelllipodia like fine protrusions appeared/ disappeared in cell membrane of bladder cancer cells.

protrusions appeared or disappeared on the cell membrane of bladder cancer cells. Urothelial cells did not show any protrusion on their cell membrane with time.

6.3.3. Hamming Distance Analysis

Hamming distance calculated the change of each and every pixel inside a cell body. This simple metric took into account the whole cell body change reflecting the overall effect of EGFR binding on both type of cells. Higher cell motility produced higher alteration in pixel values. On nanotextured anti-EGFR aptamer modified substrate bladder cancer cells showed higher Hamming distance value than urothelial cells. Average of total Hamming distance was 99110.3 a.u. (S.D.=33785 a.u.) for bladder cancer cells, and 43966.4 a.u. (S.D.=17848.02 a.u.) for urothelial cells. In Fig. 6-2(a), two tailed *t*-test showed the values are significantly different (p-value < 0.01).

6.3.4. Hausdorff Distance Analysis

Hausdorff distance calculated the minute change among two datasets. The datasets here are coordinates of cell contour in two consecutive images. As cells were changing shape, cell contour was changing position. Hausdorff distance value reflected how each and every point on cell contour changed their position with respect to previous position over time. In Fig. 6-2(b) average of total Hausdorff distance for bladder cancer cell is 282.3 a.u. (S.D.= 67.4 a.u.) and for urothelial cell is 144.1 a.u. (S.D.= 39.7 a.u.). Statistical difference of Hausdorff distance between urothelial and bladder cancer cells is significant (p-value < 0.01).

6.3.5. Mahalanobis Distance Analysis

Mahalanobis distance compared the covariance between cell contours of two successive cell shapes and provided the course shape change. Bladder cancer cells were constantly changing shape and showing high Mahalanobis distance values with time than urothelial cells. In Fig. 6-2(c), average of total Mahalanobis distance for bladder cancer cells is 0.77 a.u. (S.D.= 0.30 a.u.) and urothelial cells is 0.41 a.u. (S.D.= 0.14 a.u.). Two tailed *t*-test confirmed significant difference between two cell types on nanotextured aptamer functionalized substrate (p-value < 0.01).

Bladder cancer cells have 125.4% higher Hamming distance, 95.9% higher Hausdorff distance and 86.81% higher Mahalanobis distance than healthy urothelial cells. Three distance matrices signify three features that we considered to discriminate cell shape change between bladder cancer and urothelial cells. Hamming distance considered cell body, Hausdorff distance calculated precise contour change and Mahalanobis distance measured course contour change. Cells bound with anti-EGFR aptamer tethered with nanotextured substrate sometimes moved or rotated from initial position a little with time. Calculation based on cell body was more accurate compared with calculation based on cell contour. On the other hand cell contour based analysis was straighforward and eliminated the probably error derived from cell spreading over surface with time. Hausdorff distance was extremely sensitive to shape change with a downside of overcalculating subtle cell movement. Mahalanobis distance resolved this problem with course calculation of cell contour change. Overall, three features of cell shape change was calculated with three distance matrices and when combined they can provide an

effective discriminating feature space for detecting bladder cancer cells from healthy urothelial cells.

6.3.6. Size Comparison of Cells in Patient Urine Sample

Patient urine sample was collected, filtered and suspended on nanotextured anti-EGFR aptamer functionalized substrate. The suspension is shown in Fig. 6-3(a). Different kinds of cells having different size were observed and compared with a standard urinalysis slide. Normal urine contains epithelial cells, sometimes red bloods cells (RBCs), lipid droplets, salt and acid crystals, microorganisms and contamination like mucus and starch or fatty casts [150]. Among epithelial cells urothelial aka transitional epithelial cells are frequently present in urine and have the diameter of 20-30 μm. Another type of epithelial cell is squamous epithelial cells which are easily recognized from their large and flat size (diameter 30-50 μm) [150]. RBCs in urine have the diameter of 6.2-8.2 μm [151]. They are easily recognized from their smaller size, biconcave disk-shape. RBCs are crenellated in hypertonic urine for higher external pressure and swelled in hypotonic urine for higher internal pressure [150]. Their size, shape and crenelated feature make them easily distinguishable.

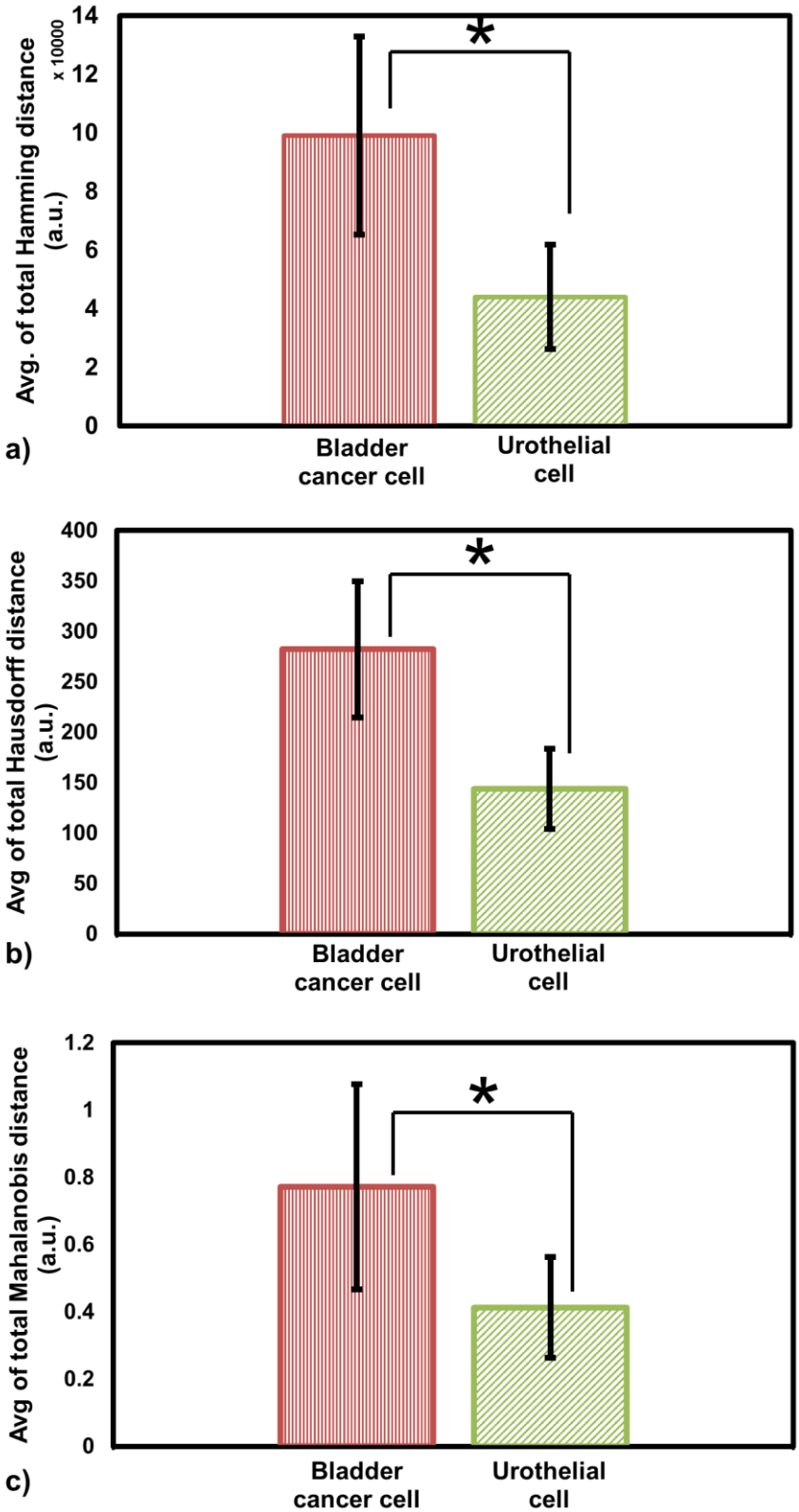

Figure 0-2: Shape dissimilarity analysis using a) Hamming distance *, $p < 0.01$; b) Hausdorff distance *, $p < 0.01$ and c) Mahalanobis distance *, $p < 0.01$ (n=81 cells). Distance matrix analysis clearly shows bladder cancer cells show higher morphological change than healthy urothelial cells.

For convenience in analysis we eliminated some cells from patient urine sample. RBCs were easily eliminated for their smaller size and shape. The cells larger than 30 µm were recognized to be squamous epithelial cells. The cast and contaminations were irregular in shape which were easily recognizable. That left us with urothelial and probable bladder cancer cells in patient urine sample. From our previous experimentation with bladder cancer and urothelial cell lines we presented the distribution of diameter in Fig. 6-3(b)(I-II), We observed bladder cancer cells and urothelial cells frequently had diameter between 10-25 µm. The cells having diameter in the range of 10-25 µm were included in subsequent analysis.

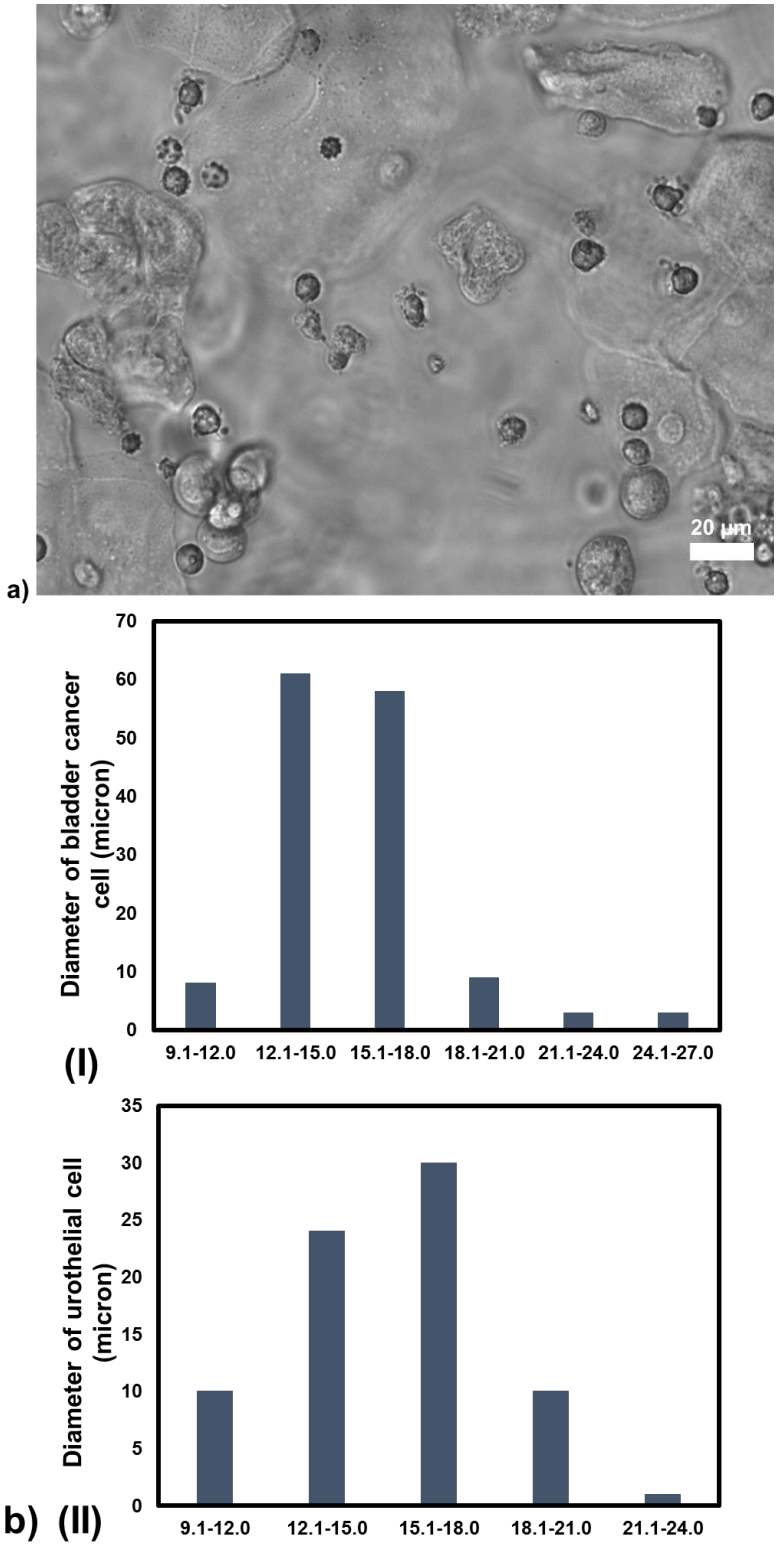

Figure 0-3: a) Bladder cancer patient urine sample suspended on anti-EGFR coated nanotextured glass substrate. Different kinds of cells and contamination are seen. b) Distribution of diameter of (I) bladder cancer cells and (II) urothelial cells are presented from our previous observation with cell lines. Both types of cells frequently showed diameter between 10-25 µm. Patient urine cells which had diameter inside the range 10-25 µm were considered for subsequent analysis.

6.3.7. Discrimination of Bladder Cancer Cells in Patient Urine Sample

Patient urine cells having diameter between 10-25 µm were selected for further analysis. These selected cells could be bladder cancer cells or normal healthy urothelial cells. We already analyzed the healthy urothelial and bladder cancer cell lines using distance matrices. Same calculations were done with selected patient urine cells. The distance profiles of cell lines and selected patient urine cells were compared in Fig. 6-4(a-c).

In Fig. 6-4 a)(I), b)(I), and c)(I), distance profiles of bladder cancer and urothelial cell lines are shown. Bladder cancer cells and urothelial cells occupied distinguishably separate areas (inside circle). Urothelial cells occupied areas with low distance values and bladder cancer cells occupied areas with high distance values. Bladder cancer cells in urine highly vary in maturity and certainly not all cells would show high distance values practically. In clinical samples, we would expect the area occupied by bladder cancer cells to be broader and overlapping with some area of healthy cells. But we expected some cancer cells would show high distance values and hence easily distinguishable. In Fig. 6-4 a)(II-III), b)(II-III) and c)(II-III), distance profiles of patient urine cells are shown. Using the previously established area in Fig. 6-4 a)(I), b)(I), and c)(I) (inside the circle), we extrapolated bladder cancer cells from patient urine samples. For robust detection we considered all three distance matrices and the distance profiles confirmed that at least 2 and 11 cells were cancerous in sample 1 and 2 respectively. Agility of cytoskeletal structure of cancer cells was enhanced on nanotextured aptamer modified substrate which resulted in vigorous morphology change. Distance profiles based on this cell modality could be effectively used as a cellular biomarker for detecting bladder cancer cells from urine samples.

For combined detection of bladder cancer cells from patient urine sample, three distance profiles are plotted together in Fig. 6-5. The cells of patient urine sample are localised in the region where bladder cancer cell population resides. It depicts the significance of high distance profile of bladder cancer cells as a potential cellular biomarker for detection.

Detecting cancer cells from urine sample is critical for early detection of high grade bladder cancer. Our nanotextured substrate proved to be extremely effective in detecting bladder cancer cells based on their distance profiles resulting from higher cell motility triggered by higher EGFR-aptamer binding. Combination of functionalized nanotextured platform with distance matrix analysis algorithm has proved to be an innovative strategy for detecting bladder cancer cells from patient urine sample in a simple and economic setting.

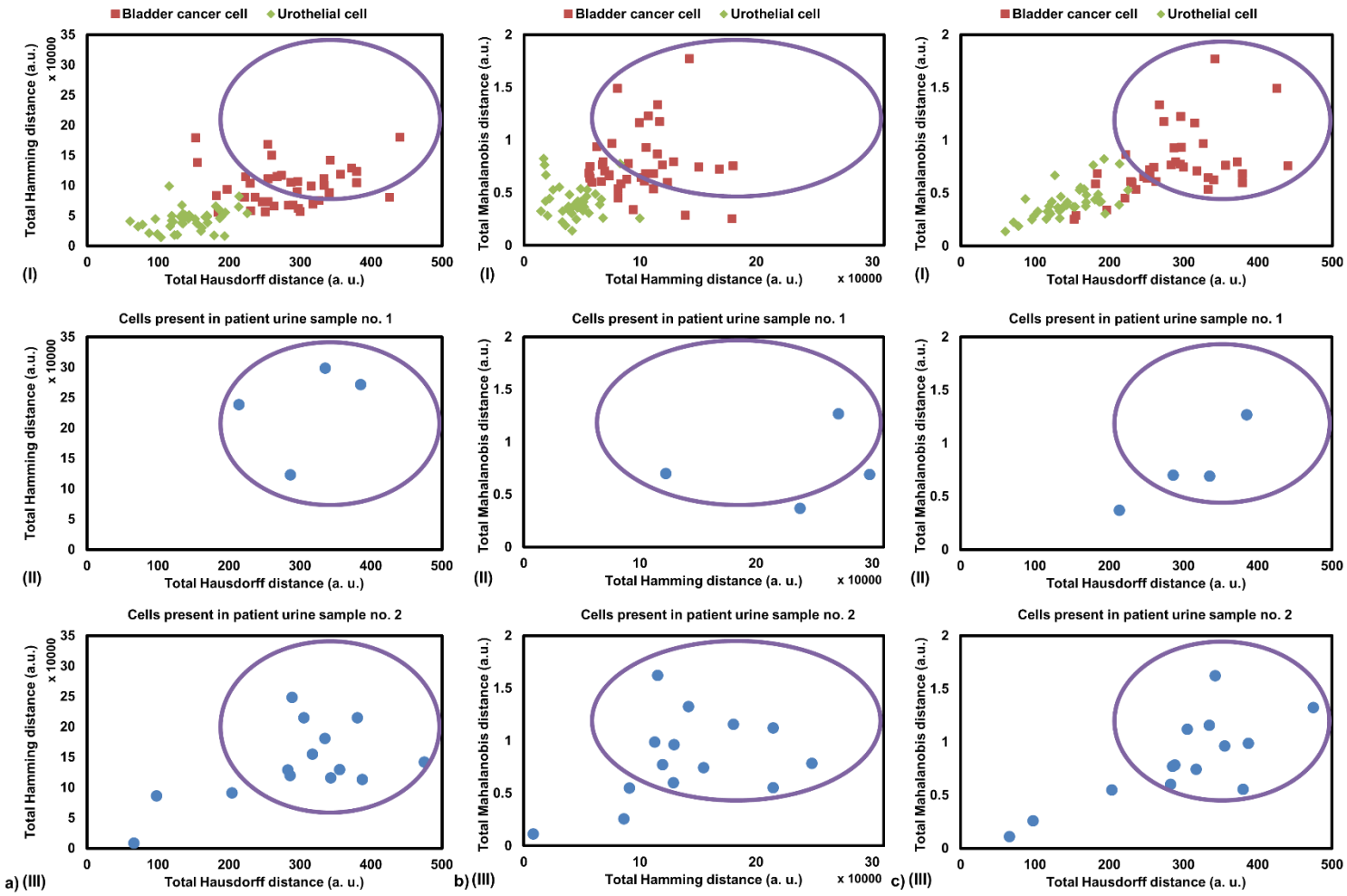

Figure 0-4: Distance matrix analysis of patient urine cells and comparison of distance profiles with cell lines after attachment on nanotextured aptamer functionalized substrate. a) Hamming and Hausdorff distance profiles for (I) bladder cancer and urothelial cell lines. (II) cells present in patient urine sample 1 (III) cells present in patient urine sample 2. b) Mahalanobis and Hamming distance profiles for (I) bladder cancer and urothelial cell lines. (II) cells present in patient urine sample 1 (III) cells present in patient urine sample 2. c) Mahalanobis and Hausdorff distance profiles for (I) bladder cancer and urothelial cell lines. (II) cells present in patient urine sample 1 (III) cells present in patient urine sample 2. a)(I), b)(I), and c)(I) show distinguishably separate areas for bladder cancer and urothelial cell lines. The areas with high distance profiles(inside circle) were established as the probable area for cancer cell population in patient urine sample. In a)(II-III), b)(II-III), and c)(II-III), some cells are located in high distance profile zone (inside circle) and are detected as bladder cancer cells.

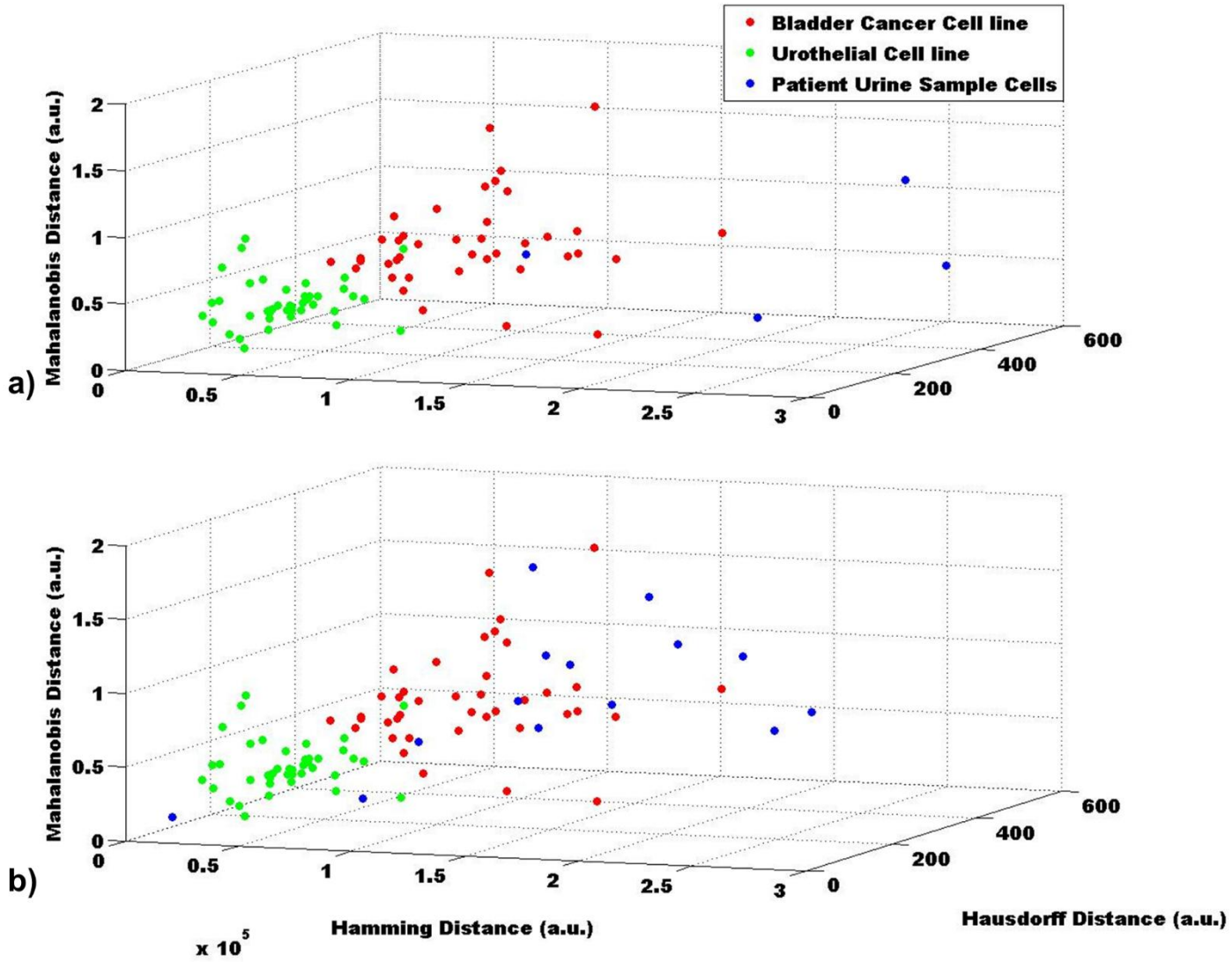

Figure 0-5: Three distance profiles combined for bladder cancer cells, urothelial cells and cells from patient urine sample; a) patient urine sample no. 1 and b) patient urine sample no. 2. The concordance of the locality of patient urine sample cells with that of bladder cancer cells depicts the significance of high distance profile of bladder cancer cells as a potential cellular biomarker.

6.4. Conclusions

We have presented an unique platform to detect bladder cancer cells from patient urine sample based on their distinguishable distance profiles on anti-EGFR aptamer modified nanotextured substrates. This technique is non-invasive and label free. Anti-EGFR aptamer provided selectivity between healthy and cancer cells. EGFR binding with anti-

EGFR aptamer stimulated cell cytoskeleton flexibility in cancer cells. We successfully detected bladder cancer cells from other types of cells from urine of a bladder cancer patient. High sensitivy of the technique can be ensured by suspending the sample on a bigger substrate and using a stepper microscope to record images in all locations on the substrate. This technique is economical as there is no need to use expensive sensing transducers or tedious methods for fabrication. Fabrication of uniformly nanotextured substrate is simple and easy. The functionalization process is highly standardized with high capture efficiency and widely accepted. This capture platform coupled with distance analysis method has the potential to be developed into an inexpensive and efficient point of care device to detect bladder cancer cells from collected urine and determine cancer in a person.

References

1. Baccelli, I., et al., *Identification of a population of blood circulating tumor cells from breast cancer patients that initiates metastasis in a xenograft assay.* Nature biotechnology, 2013. **31**(6): p. 539-544.
2. Hodgkinson, C.L., et al., *Tumorigenicity and genetic profiling of circulating tumor cells in small-cell lung cancer.* Nature medicine, 2014. **20**(8): p. 897-903.
3. Steen, S., et al. *Circulating tumor cells in melanoma: a review of the literature and description of a novel technique*. in *Baylor University Medical Center. Proceedings*. 2008. Baylor University Medical Center.
4. Allard, W.J., et al., *Tumor cells circulate in the peripheral blood of all major carcinomas but not in healthy subjects or patients with nonmalignant diseases.* Clinical Cancer Research, 2004. **10**(20): p. 6897-6904.
5. Krebs, M.G., et al., *Evaluation and prognostic significance of circulating tumor cells in patients with non–small-cell lung cancer.* Journal of clinical oncology, 2011. **29**(12): p. 1556-1563.
6. Cristofanilli, M., et al., *Circulating tumor cells, disease progression, and survival in metastatic breast cancer.* New England Journal of Medicine, 2004. **351**(8): p. 781-791.
7. De Bono, J.S., et al., *Circulating tumor cells predict survival benefit from treatment in metastatic castration-resistant prostate cancer.* Clinical Cancer Research, 2008. **14**(19): p. 6302-6309.
8. Cohen, S., et al., *Prognostic significance of circulating tumor cells in patients with metastatic colorectal cancer.* Annals of Oncology, 2009. **20**(7): p. 1223-1229.
9. Alix-Panabières, C. and K. Pantel, *Challenges in circulating tumour cell research.* Nature Reviews Cancer, 2014. **14**(9): p. 623-631.
10. Mocellin, S., et al., *The prognostic value of circulating tumor cells in patients with melanoma: a systematic review and meta-analysis.* Clinical cancer research, 2006. **12**(15): p. 4605-4613.
11. Wiedswang, G. and B. Naume, *Can detection of circulating tumor cells in peripheral blood provide prognostic data in breast cancer?* Nature Clinical Practice Oncology, 2007. **4**(3): p. 154-155.
12. Nole, F., et al., *Variation of circulating tumor cell levels during treatment of metastatic breast cancer: prognostic and therapeutic implications.* Annals of Oncology, 2007: p. mdm558.
13. Rolle, A., et al., *Increase in number of circulating disseminated epithelial cells after surgery for non-small cell lung cancer monitored by MAINTRAC® is a predictor for relapse: a preliminary report.* World journal of surgical oncology, 2005. **3**(1): p. 18.
14. Society, A.C., *Breast Cancer Facts & Figures 2013-2014*. 2013, American Cancer Society, Inc.: Atlanta.
15. O'Shaughnessy, J., *Extending survival with chemotherapy in metastatic breast cancer.* The oncologist, 2005. **10**(Supplement 3): p. 20-29.
16. Society, A.C., *NCI SEER data analysis 2000-2005*. American Cancer Society, Inc.
17. Siegel, R.L., K.D. Miller, and A. Jemal, *Cancer statistics, 2016.* CA: a cancer journal for clinicians, 2016. **66**(1): p. 7-30.
18. Holmang, S., et al., *The relationship among multiple recurrences, progression and prognosis of patients with stages Ta and T1 transitional cell cancer of the bladder followed for at least 20 years.* The Journal of urology, 1995. **153**(6): p. 1823-1827.
19. Weissleder, R., *Scaling down imaging: molecular mapping of cancer in mice.* Nature reviews. Cancer, 2002. **2**(1): p. 11.
20. Jaffer, F.A. and R. Weissleder, *Molecular imaging in the clinical arena.* Jama, 2005. **293**(7): p. 855-862.

21. Guller, U., et al., *Selective axillary surgery in breast cancer patients based on positron emission tomography with 18 F-fluoro-2-deoxy-D-glucose: not yet!* Breast cancer research and treatment, 2002. **71**(2): p. 171-173.
22. Quon, A. and S.S. Gambhir, *FDG-PET and beyond: molecular breast cancer imaging.* Journal of clinical oncology, 2005. **23**(8): p. 1664-1673.
23. Swennenhuis, J.F., et al., *Characterization of circulating tumor cells by fluorescence in situ hybridization.* Cytometry Part A, 2009. **75**(6): p. 520-527.
24. Rodgers, M., et al., *Diagnostic tests and algorithms used in the investigation of haematuria: systematic reviews and economic evaluation.* 2006.
25. Descotes, F., et al., *Non-invasive prediction of recurrence in bladder cancer by detecting somatic TERT promoter mutations in urine.* British Journal of Cancer, 2017.
26. Miremami, J. and N. Kyprianou, *The promise of novel molecular markers in bladder cancer.* International journal of molecular sciences, 2014. **15**(12): p. 23897-23908.
27. Sánchez-Carbayo, M., et al., *Urinary tissue polypeptide-specific antigen for the diagnosis of bladder cancer.* Urology, 2000. **55**(4): p. 526-532.
28. Sánchez-Carbayo, M., et al., *Initial evaluation of the new urinary bladder cancer rapid test in the detection of transitional cell carcinoma of the bladder.* Urology, 1999. **54**(4): p. 656-661.
29. Baard, J., et al., *Diagnostic dilemmas in patients with upper tract urothelial carcinoma.* Nature Reviews Urology, 2016.
30. Karakiewicz, P.I., et al., *Institutional variability in the accuracy of urinary cytology for predicting recurrence of transitional cell carcinoma of the bladder.* BJU international, 2006. **97**(5): p. 997-1001.
31. Owens, C.L., et al., *A review of reporting systems and terminology for urine cytology.* Cancer cytopathology, 2013. **121**(1): p. 9-14.
32. Bastacky, S., et al., *The accuracy of urinary cytology in daily practice.* Cancer Cytopathology, 1999. **87**(3): p. 118-128.
33. Ramakumar, S., et al., *Comparison of screening methods in the detection of bladder cancer.* The Journal of urology, 1999. **161**(2): p. 388-394.
34. Warde, N., *Diagnosis: Combined urine assays improve detection of urothelial cancer.* Nature Reviews Urology, 2011. **8**(5): p. 233-233.
35. Koss, L., et al., *Diagnostic value of cytology of voided urine.* Acta cytologica, 1985. **29**(5): p. 810-816.
36. Piaton, E., et al., *Cost efficiency analysis of modern cytocentrifugation methods versus liquid based (Cytyc Thinprep®) processing of urinary samples.* Journal of clinical pathology, 2004. **57**(11): p. 1208-1212.
37. Bassi, P., et al., *Non-invasive diagnostic tests for bladder cancer: a review of the literature.* Urologia internationalis, 2005. **75**(3): p. 193-200.
38. Fontaniere, B., et al., *Quality criteria in urinary cytology for tumor diagnosis.* Progres en urologie: journal de l'Association francaise d'urologie et de la Societe francaise d'urologie, 2001. **11**(5): p. 867-875.
39. Caraway, N.P. and R.L. Katz, *A review on the current state of urine cytology emphasizing the role of fluorescence in situ hybridization as an adjunct to diagnosis.* Cancer cytopathology, 2010. **118**(4): p. 175-183.
40. Junker, K., et al., *Multicolor fluorescence in situ hybridization (M-FISH) on cells from urine for the detection of bladder cancer.* Cytogenetic and genome research, 2006. **114**(3-4): p. 279-283.
41. Halling, K.C., et al., *A comparison of cytology and fluorescence in situ hybridization for the detection of urothelial carcinoma.* The Journal of urology, 2000. **164**(5): p. 1768-1775.

42. Kamat, A.M., et al., *ICUD-EAU International Consultation on Bladder Cancer 2012: screening, diagnosis, and molecular markers.* European urology, 2013. **63**(1): p. 4-15.
43. Mowatt, G., et al., *Systematic review of the clinical effectiveness and cost-effectiveness of photodynamic diagnosis and urine biomarkers (FISH, ImmunoCyt, NMP22) and cytology for the detection and follow-up of bladder cancer.* 2010.
44. Lotan, Y. and C.G. Roehrborn, *Sensitivity and specificity of commonly available bladder tumor markers versus cytology: results of a comprehensive literature review and meta-analyses.* Urology, 2003. **61**(1): p. 109-118.
45. Raitanen, M.-P. and F. Group, *The role of BTA stat Test in follow-up of patients with bladder cancer: results from FinnBladder studies.* World journal of urology, 2008. **26**(1): p. 45-50.
46. Raitanen, M.-P., et al., *Analysis of false-positive BTA STAT test results in patients followed up for bladder cancer.* Urology, 2001. **57**(4): p. 680-684.
47. Rosser, C.J., et al., *Urinary protein biomarker panel for the detection of recurrent bladder cancer.* Cancer Epidemiology and Prevention Biomarkers, 2014.
48. Chou, R., et al., *Urinary biomarkers for diagnosis of bladder cancer.* Annals of internal medicine, 2015. **163**(12): p. 922-931.
49. Herr, H., *The natural history of a T1 bladder cancer: life-long tumour diathesis.* BJU international, 1999. **84**: p. 1102-1103.
50. van der Poel, H.G. and F.M. Debruyne, *Can biological markers replace cystoscopy? An update.* Current opinion in urology, 2001. **11**(5): p. 503-509.
51. Hwang, E.C., et al., *Use of the NMP22 BladderChek test in the diagnosis and follow-up of urothelial cancer: a cross-sectional study.* Urology, 2011. **77**(1): p. 154-159.
52. Saeb-Parsy, K., et al., *Diagnosis of bladder cancer by immunocytochemical detection of minichromosome maintenance protein-2 in cells retrieved from urine.* British journal of cancer, 2012. **107**(8): p. 1384.
53. Mendelsohn, J., *EGF receptors as a target for cancer therapy.* Transactions of the American Clinical and Climatological Association, 2004. **115**: p. 249.
54. Maheswaran, S., et al., *Detection of mutations in EGFR in circulating lung-cancer cells.* New England Journal of Medicine, 2008. **359**(4): p. 366-377.
55. Franovic, A., et al., *Translational up-regulation of the EGFR by tumor hypoxia provides a nonmutational explanation for its overexpression in human cancer.* Proceedings of the National Academy of Sciences, 2007. **104**(32): p. 13092-13097.
56. Islam, M., et al., *Electrical Profiling and Aptamer Functionalized Nanotextured Surface in a Single Biochip for the Detection of Tumor Cells.*
57. Islam, M., et al., *Effects of nanotexture on electrical profiling of single tumor cell and detection of cancer from blood in microfluidic channels.* Scientific reports, 2015. **5**.
58. Carpenter, G. and S. Cohen, *Epidermal growth factor.* Annual review of biochemistry, 1979. **48**(1): p. 193-216.
59. Carpenter, G., *The biochemistry and physiology of the receptor-kinase for epidermal growth factor.* Molecular and cellular endocrinology, 1983. **31**(1): p. 1-19.
60. Cai, Z., et al., *Relationship between induction of phosphorylated H2AX and survival in breast cancer cells exposed to 111In-DTPA-hEGF.* Journal of Nuclear Medicine, 2008. **49**(8): p. 1353-1361.
61. Mellon, K., et al., *Bladder cancer: long-term outcome related to epidermal growth factor receptor status in bladder cancer.* The Journal of urology, 1995. **153**(3): p. 919-925.
62. Neal, D., et al., *Epidermal-growth-factor receptors in human bladder cancer: comparison of invasive and superficial tumours.* The Lancet, 1985. **325**(8425): p. 366-368.

63. Kramer, C., et al., *Heparin-binding epidermal growth factor-like growth factor isoforms and epidermal growth factor receptor/ErbB1 expression in bladder cancer and their relation to clinical outcome.* Cancer, 2007. **109**(10): p. 2016-2024.
64. Bue, P., et al., *Expression of epidermal growth factor receptor in urinary bladder cancer metastases.* The Journal of Urology, 1998. **160**(5): p. 1937-1938.
65. Colquhoun, A.J. and J.K. Mellon, *Epidermal growth factor receptor and bladder cancer.* Postgraduate medical journal, 2002. **78**(924): p. 584-589.
66. Donato, N.J., et al., *Tumor necrosis factor modulates epidermal growth factor receptor phosphorylation and kinase activity in human tumor cells. Correlation with cytotoxicity.* Journal of Biological Chemistry, 1989. **264**(34): p. 20474-20481.
67. Ishikawa, J., et al., *EGF stimulates anchorage-independent growth of a human bladder carcinoma cell line (KU1) with an amplified and over-expressed EGF receptor gene.* International journal of cancer, 1989. **44**(6): p. 1000-1004.
68. Bunka, D.H. and P.G. Stockley, *Aptamers come of age–at last.* Nature Reviews Microbiology, 2006. **4**(8): p. 588-596.
69. Sullenger, B.A. and E. Gilboa, *Emerging clinical applications of RNA.* Nature, 2002. **418**(6894): p. 252-258.
70. Reuben, J.M., et al., *The role of circulating tumor cells in breast cancer diagnosis and prediction of therapy response.* Expert opinion on medical diagnostics, 2008. **2**(4): p. 339-348.
71. Urtishak, S., et al., *Clinical utility of circulating tumor cells: a role for monitoring response to therapy and drug development.* 2008.
72. Zhang, L., et al., *Meta-analysis of the prognostic value of circulating tumor cells in breast cancer.* Clinical cancer research, 2012. **18**(20): p. 5701-5710.
73. Losanoff, J.E., et al., *Can mitochondrial DNA mutations in circulating white blood cells and serum be used to detect breast cancer?* The Breast, 2008. **17**(5): p. 540-542.
74. Zieglschmid, V., C. Hollmann, and O. Böcher, *Detection of disseminated tumor cells in peripheral blood.* Critical reviews in clinical laboratory sciences, 2005. **42**(2): p. 155-196.
75. Kahn, H.J., et al., *Enumeration of circulating tumor cells in the blood of breast cancer patients after filtration enrichment: correlation with disease stage.* Breast cancer research and treatment, 2004. **86**(3): p. 237-247.
76. Pelkey, T., H. Frierson, and D. Bruns, *Molecular and immunological detection of circulating tumor cells and micrometastases from solid tumors.* Clinical chemistry, 1996. **42**(9): p. 1369-1381.
77. Krivacic, R.T., et al., *A rare-cell detector for cancer.* Proceedings of the National Academy of Sciences of the United States of America, 2004. **101**(29): p. 10501-10504.
78. Yagata, H., et al., *Evaluation of circulating tumor cells in patients with breast cancer: multi-institutional clinical trial in Japan.* International journal of clinical oncology, 2008. **13**(3): p. 252-256.
79. Schröder, C.P., et al., *Detection of micrometastatic breast cancer by means of real time quantitative RT-PCR and immunostaining in perioperative blood samples and sentinel nodes.* International journal of cancer, 2003. **106**(4): p. 611-618.
80. Mattano, L.A., T.J. Moss, and S.G. Emerson, *Sensitive detection of rare circulating neuroblastoma cells by the reverse transcriptase-polymerase chain reaction.* Cancer research, 1992. **52**(17): p. 4701-4705.
81. Dawood, S., et al., *Circulating tumor cells in metastatic breast cancer.* Cancer, 2008. **113**(9): p. 2422-2430.
82. Szatanek, R., et al., *Detection of isolated tumour cells in the blood and bone marrow of patients with gastric cancer by combined sorting, isolation and determination of MAGE-1,-2 mRNA expression.* Oncology reports, 2008. **19**(4): p. 1055-1060.

83. Moreno, J.G., et al., *Changes in circulating carcinoma cells in patients with metastatic prostate cancer correlate with disease status.* Urology, 2001. **58**(3): p. 386-392.
84. Nagrath, S., et al., *Isolation of rare circulating tumour cells in cancer patients by microchip technology.* Nature, 2007. **450**(7173): p. 1235-1239.
85. Adams, A.A., et al., *Highly efficient circulating tumor cell isolation from whole blood and label-free enumeration using polymer-based microfluidics with an integrated conductivity sensor.* Journal of the American Chemical Society, 2008. **130**(27): p. 8633.
86. Yu, M., et al., *Circulating tumor cells: approaches to isolation and characterization.* The Journal of cell biology, 2011. **192**(3): p. 373-382.
87. Liliensiek, S.J., P. Nealey, and C.J. Murphy, *Characterization of endothelial basement membrane nanotopography in rhesus macaque as a guide for vessel tissue engineering.* Tissue Engineering Part A, 2009. **15**(9): p. 2643-2651.
88. Liotta, L., et al., *Metastatic potential correlates with enzymatic degradation of basement membrane collagen.* Nature, 1980. **284**(5751): p. 67-68.
89. Fischer, K.E., et al., *Biomimetic nanowire coatings for next generation adhesive drug delivery systems.* Nano letters, 2009. **9**(2): p. 716-720.
90. Kim, S.T., et al., *Novel streptavidin-functionalized silicon nanowire arrays for CD4+ T lymphocyte separation.* Nano letters, 2010. **10**(8): p. 2877-2883.
91. Asghar, W., et al., *Synthesis of nano-textured biocompatible scaffolds from chicken eggshells.* Nanotechnology, 2012. **23**(47): p. 475601.
92. Thapa, A., et al., *Nano-structured polymers enhance bladder smooth muscle cell function.* Biomaterials, 2003. **24**(17): p. 2915-2926.
93. Miller, D.C., et al., *Endothelial and vascular smooth muscle cell function on poly (lactic-co-glycolic acid) with nano-structured surface features.* Biomaterials, 2004. **25**(1): p. 53-61.
94. Wan, Y., et al., *Surface-immobilized aptamers for cancer cell isolation and microscopic cytology.* Cancer research, 2010. **70**(22): p. 9371-9380.
95. Mahmood, M.A.I., et al., *One-step tumor detection from dynamic morphology tracking on aptamer-grafted surfaces.* Technology, 2015. **3**(04): p. 194-200.
96. Sethian, J.A., *Analysis of flame propagation*. 1982, Lawrence Berkeley Lab., CA (USA).
97. Huttenlocher, D.P., G.A. Klanderman, and W.J. Rucklidge, *Comparing images using the Hausdorff distance.* IEEE Transactions on pattern analysis and machine intelligence, 1993. **15**(9): p. 850-863.
98. Mahalanobis, P.C. *On the Generalized Distance in Statistics*. in *Proceedings of National Institute of Sciences*. 1936. India.
99. Wells, A., *EGF receptor.* The international journal of biochemistry & cell biology, 1999. **31**(6): p. 637-643.
100. Alberts, B., et al., *Molecular Biology of the Cell*. 4th ed. 2002, New York: Garland Science.
101. Parent, C.A. and P.N. Devreotes, *A cell's sense of direction.* Science, 1999. **284**(5415): p. 765-770.
102. Van Leeuwen, F.N., et al., *Rac regulates phosphorylation of the myosin-II heavy chain, actinomyosin disassembly and cell spreading.* Nature Cell Biology, 1999. **1**(4): p. 242-248.
103. Anselme, K., *Osteoblast adhesion on biomaterials.* Biomaterials, 2000. **21**(7): p. 667-681.
104. Mogilner, A. and G. Oster, *Cell motility driven by actin polymerization.* Biophysical journal, 1996. **71**(6): p. 3030-3045.
105. Wang, W., et al., *Identification and testing of a gene expression signature of invasive carcinoma cells within primary mammary tumors.* Cancer research, 2004. **64**(23): p. 8585-8594.
106. Normanno, N., et al., *Epidermal growth factor receptor (EGFR) signaling in cancer.* Gene, 2006. **366**(1): p. 2-16.
107. Wan, Y., et al., *Nanotextured substrates with immobilized aptamers for cancer cell isolation and cytology.* Cancer, 2012. **118**(4): p. 1145-1154.

108. Mahmood, M.A.I., et al., *Micro+ nanotexturing of substrates to enhance ligand-assisted cancer cell isolation.* Nanotechnology, 2014. **25**(47): p. 475102.
109. Jaccard, P., *Distribution de la flore alpine dans le bassin des Dranses et dans quelques régions voisines.* Bull. Soc. Vaud. Sci. Nat., 1901. **37**: p. 241-272.
110. Nosonovsky, M. and B. Bhushan, *Biologically inspired surfaces: broadening the scope of roughness.* Advanced Functional Materials, 2008. **18**(6): p. 843-855.
111. Scotchford, C.A., et al., *Protein adsorption and human osteoblast-like cell attachment and growth on alkylthiol on gold self-assembled monolayers.* Journal of biomedical materials research, 2002. **59**(1): p. 84-99.
112. Ferretti, S., et al., *Self-assembled monolayers: a versatile tool for the formulation of bio-surfaces.* TrAC Trends in Analytical Chemistry, 2000. **19**(9): p. 530-540.
113. John, P.M.S., et al., *Preferential glial cell attachment to microcontact printed surfaces.* Journal of neuroscience methods, 1997. **75**(2): p. 171-177.
114. Zreiqat, H. and C.R. Howlett, *Titanium substrata composition influences osteoblastic phenotype: in vitro study.* Journal of biomedical materials research, 1999. **47**(3): p. 360-366.
115. Zreiqat, H., P. Evans, and C.R. Howlett, *Effect of surface chemical modification of bioceramic on phenotype of human bone-derived cells.* Journal of Biomedical Materials Research Part A, 1999. **44**(4): p. 389-396.
116. Healy, K.E., et al., *Kinetics of bone cell organization and mineralization on materials with patterned surface chemistry.* Biomaterials, 1996. **17**(2): p. 195-208.
117. Chen, P., et al., *Epidermal growth factor receptor-mediated cell motility: phospholipase C activity is required, but mitogen-activated protein kinase activity is not sufficient for induced cell movement.* The Journal of cell biology, 1994. **127**(3): p. 847-857.
118. Chen, P., K. Gupta, and A. Wells, *Cell movement elicited by epidermal growth factor receptor requires kinase and autophosphorylation but is separable from mitogenesis.* The Journal of cell biology, 1994. **124**(4): p. 547-555.
119. Chen, P., J.E. Murphy-Ullrich, and A. Wells, *A role for gelsolin in actuating epidermal growth factor receptor-mediated cell motility.* Journal of Cell Biology, 1996. **134**(3): p. 689-698.
120. Suresh, S., J. Mills, and M. Dao. *Single-cell nanomechanics and human disease states*. in *ABSTRACTS OF PAPERS OF THE AMERICAN CHEMICAL SOCIETY*. 2005. AMER CHEMICAL SOC 1155 16TH ST, NW, WASHINGTON, DC 20036 USA.
121. Guck, J., et al., *Optical deformability as an inherent cell marker for testing malignant transformation and metastatic competence.* Biophysical journal, 2005. **88**(5): p. 3689-3698.
122. Suresh, S., *Biomechanics and biophysics of cancer cells.* Acta Materialia, 2007. **55**(12): p. 3989-4014.
123. Betz, T., D. Lim, and J.A. Käs, *Neuronal growth: a bistable stochastic process.* Physical review letters, 2006. **96**(9): p. 098103.
124. Hofman, P., et al., *Neutrophil F-actin and myosin but not microtubules functionally regulate transepithelial migration induced by interleukin 8 across a cultured intestinal epithelial monolayer.* European cytokine network, 1999. **10**(2): p. 227-236.
125. Baker, H.J., J.R. Lindsey, and S.H. Wesibroth, *The laboratory rat: biology and diseases*. Vol. 1. 2013: Elsevier.
126. Lele, S. and J.T. Richtsmeier, *Euclidean distance matrix analysis: A coordinate-free approach for comparing biological shapes using landmark data.* American Journal of Physical Anthropology, 1991. **86**(3): p. 415-427.
127. Anselme, K., et al., *The interaction of cells and bacteria with surfaces structured at the nanometre scale.* Acta biomaterialia, 2010. **6**(10): p. 3824-3846.

128. Teixeira, A.I., et al., *Epithelial contact guidance on well-defined micro-and nanostructured substrates.* Journal of cell science, 2003. **116**(10): p. 1881-1892.
129. Karuri, N.W., et al., *Biological length scale topography enhances cell-substratum adhesion of human corneal epithelial cells.* Journal of cell science, 2004. **117**(15): p. 3153-3164.
130. Diehl, K., et al., *Nanoscale topography modulates corneal epithelial cell migration.* Journal of Biomedical Materials Research Part A, 2005. **75**(3): p. 603-611.
131. Bunk, R., et al., *Actomyosin motility on nanostructured surfaces.* Biochemical and biophysical research communications, 2003. **301**(3): p. 783-788.
132. Johansson, F., et al., *Axonal outgrowth on nano-imprinted patterns.* Biomaterials, 2006. **27**(8): p. 1251-1258.
133. Barbucci, R., et al., *Micro and nano-structured surfaces.* Journal of Materials Science: Materials in Medicine, 2003. **14**(8): p. 721-725.
134. Hamilton, D., et al., *Articular chondrocyte passage number: influence on adhesion, migration, cytoskeletal organisation and phenotype in response to nano-and micro-metric topography.* Cell biology international, 2005. **29**(6): p. 408-421.
135. Zhu, B., et al., *Alignment of osteoblast-like cells and cell-produced collagen matrix induced by nanogrooves.* Tissue engineering, 2005. **11**(5-6): p. 825-834.
136. Fife, C., J. McCarroll, and M. Kavallaris, *Movers and shakers: cell cytoskeleton in cancer metastasis.* British journal of pharmacology, 2014. **171**(24): p. 5507-5523.
137. Hanahan, D. and R.A. Weinberg, *Hallmarks of cancer: the next generation.* cell, 2011. **144**(5): p. 646-674.
138. Karlsson, R., et al., *Rho GTPase function in tumorigenesis.* Biochimica et Biophysica Acta (BBA)-Reviews on Cancer, 2009. **1796**(2): p. 91-98.
139. Eitaki, M., et al., *Vincristine enhances amoeboid-like motility via GEF-H1/RhoA/ROCK/Myosin light chain signaling in MKN45 cells.* BMC cancer, 2012. **12**(1): p. 469.
140. Ishiwata, T., Y. Matsuda, and Z. Naito, *Nestin in gastrointestinal and other cancers: effects on cells and tumor angiogenesis.* World J Gastroenterol, 2011. **17**(4): p. 409-18.
141. Satelli, A. and S. Li, *Vimentin in cancer and its potential as a molecular target for cancer therapy.* Cellular and molecular life sciences, 2011. **68**(18): p. 3033-3046.
142. de Vicente, J.C., et al., *Focal adhesion kinase overexpression: Correlation with lymph node metastasis and shorter survival in oral squamous cell carcinoma.* Head & neck, 2013. **35**(6): p. 826-830.
143. Thiery, J.P., et al., *Epithelial-mesenchymal transitions in development and disease.* cell, 2009. **139**(5): p. 871-890.
144. Wan, Y., et al., *Velocity effect on aptamer-based circulating tumor cell isolation in microfluidic devices.* The Journal of Physical Chemistry B, 2011. **115**(47): p. 13891-13896.
145. Mansur, N., et al., *Functionalization of Nanotextured Substrates for Enhanced Identification of Metastatic Breast Cancer Cells.* Nanotechnology, 2017.
146. Liang, C., A.R. Forrest, and G.P. Wagner, *The statistical geometry of transcriptome divergence in cell-type evolution and cancer.* Nature communications, 2015. **6**: p. 6066.
147. Zheng, G.X., et al., *Massively parallel digital transcriptional profiling of single cells.* Nature communications, 2017. **8**: p. 14049.
148. Solomon, B. and C. Kingsford, *Fast search of thousands of short-read sequencing experiments.* Nature biotechnology, 2016. **34**(3): p. 300.
149. Ghaffari, P., et al., *Identifying anti-growth factors for human cancer cell lines through genome-scale metabolic modeling.* Scientific reports, 2015. **5**.
150. McClatchey, K.D., *Clinical laboratory medicine*. 2002: Lippincott Williams & Wilkins.
151. Ali, S., *Cell organisation and Function*. 2014: Pearson Education India.

Biographical Information

Nuzhat Mansur was born and raised in Dhaka, the capital of Bangladesh. She graduated as an Electrical Engineer from Bangladesh University of Engineering and Technology (BUET), Dhaka, Bangladesh in 2009. She started her PhD in University of Texas at Arlington, Arlington, Texas, USA in fall of 2011. Her research focus was detection of metastatic cancer at early stages. She worked with Nano-Bio Lab under Dr. Samir Iqbal towards developing an economic and simple early detection device for metastatic breast and bladder cancer. For her research work she won several awards from the department. She earned her PhD in summer of 2017. She is very enthusiastic to broaden her research in clinical oncology after her PhD.